Computational Investigation of Nominally-Orthogonal Pneumatic Active Flow Control for Aircraft High-Lift Systems

S.Sheida Hosseini
C.P. van Dam
Shishir Pandya (NASA Ames Research Center)
January 9, 2018

Motivation

Active Flow Control for high-lift systems

- $C_{L_{max}}$
- L/D
- Lift in the linear region

Active Flow Control (AFC)

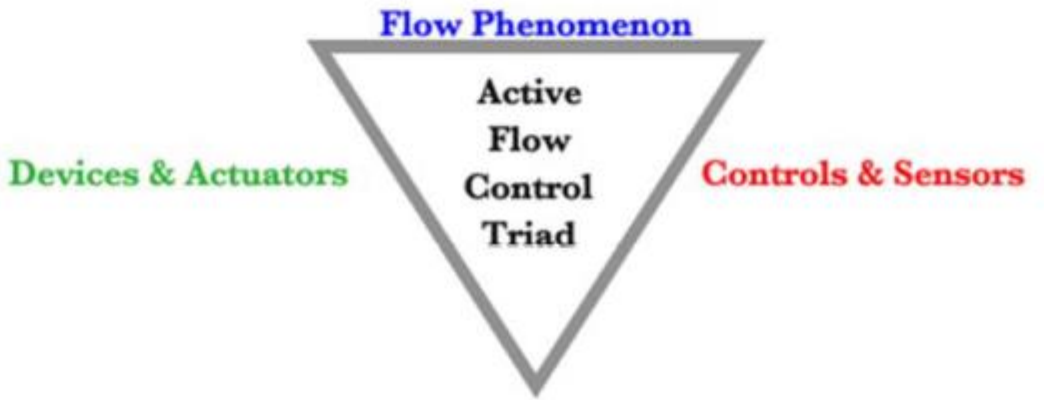

Separation Mitigation

Load Control

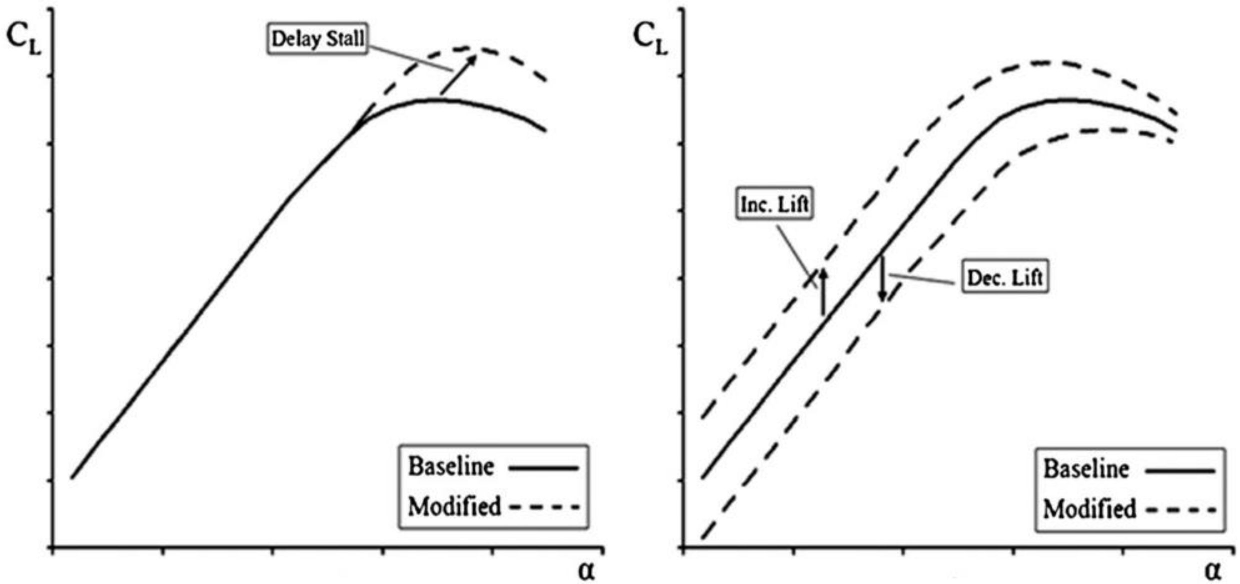

Kral 1998
Johnson et al. 2008

Load Control, Previous Work

1%c tab located at 1%c upstream of trailing edge

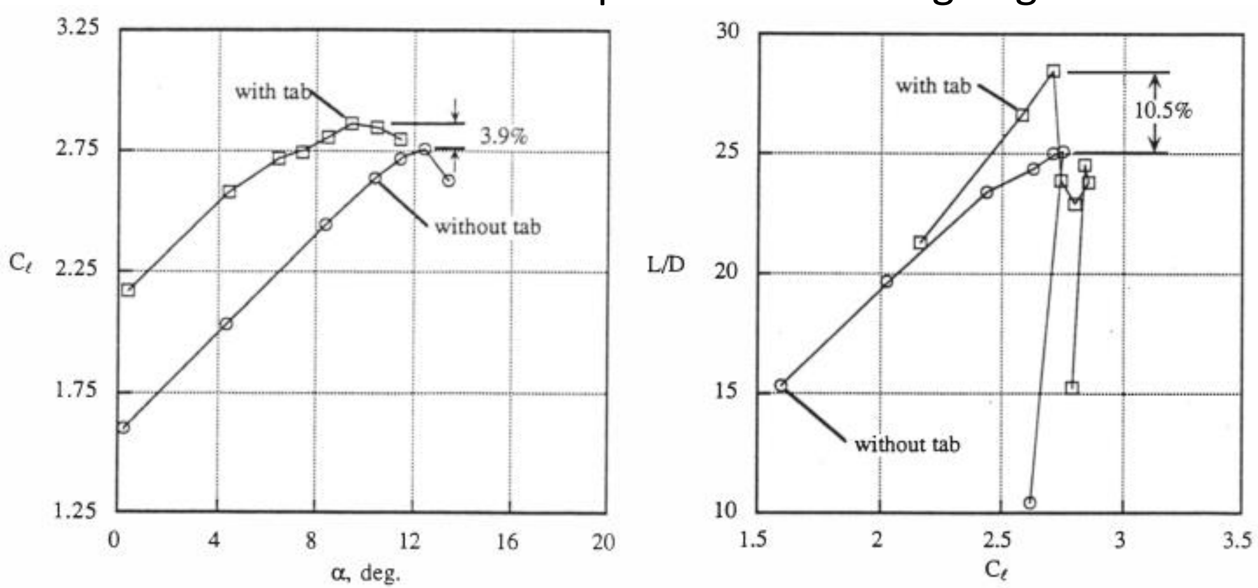

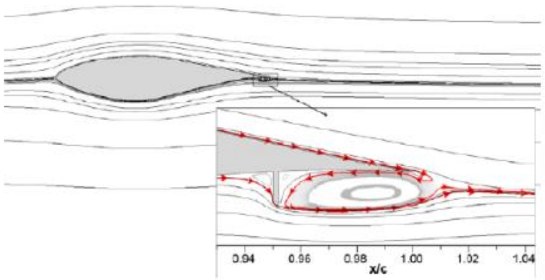

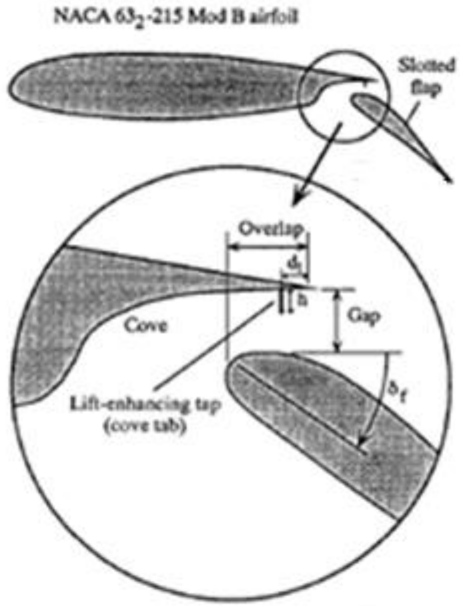

- Vertical tabs (Gurney flaps) can increase L/D
- Geometric tabs increase loads (flap weight)
- Tabs require physical space
- Tabs are not necessarily continuous
- Quick movement of tab is desirable – AFC allows rapid activation

Storms and Ross, 1995
Johnson et al. 2010

AFC Load Control, Previous Work

- No mechanical tabs, instead small jets normal to the surface
- Steady-blowing microjets: TE flow control similar to microtabs
- Experimental studies on a single-element S819 airfoil suggest a significant lift enhancement for relatively low momentum coefficient values and relative velocities, $U_{jet}/U_{\infty} = 0.5 - 1.0$

Lift coefficient versus angle of attack for S819 airfoil with active jets on upper and lower surfaces, Re = 1.0E6, Cμ = 0.0056
$U_{jet}/U_{\infty} = 0.7$

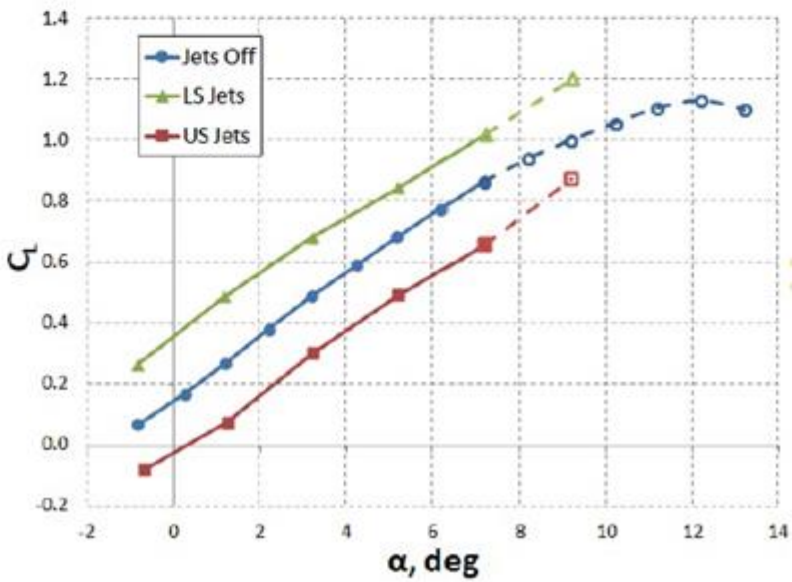

Lift coefficient versus angle of attack for jets at Re = 1.0E6 with varying Cμ

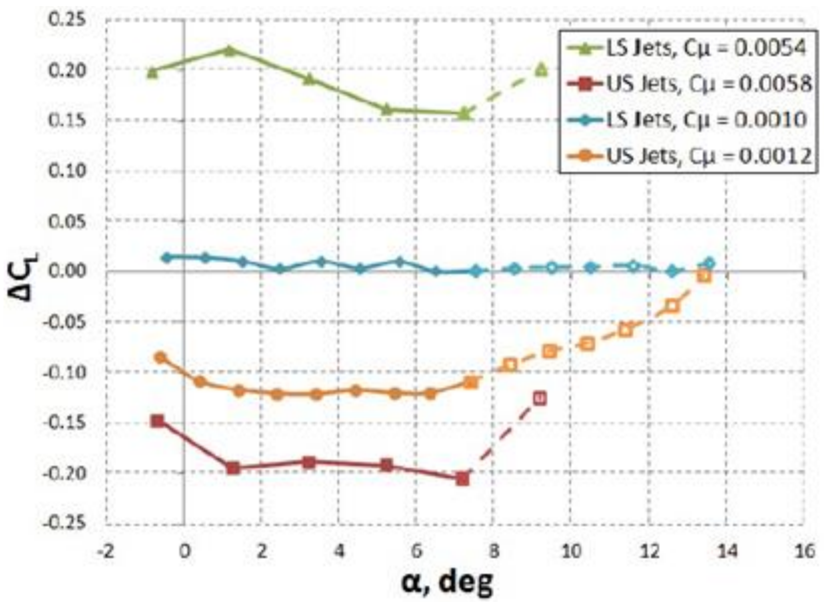

Outline

- Computational setup prior to microjet activation
  - Various grid and solver sensitivities
- Investigation of flap microjet up to date
  - Microjet vs. Microtab
  - Sensitivities of lift and drag to microjet settings
- Future work and anticipated timeline

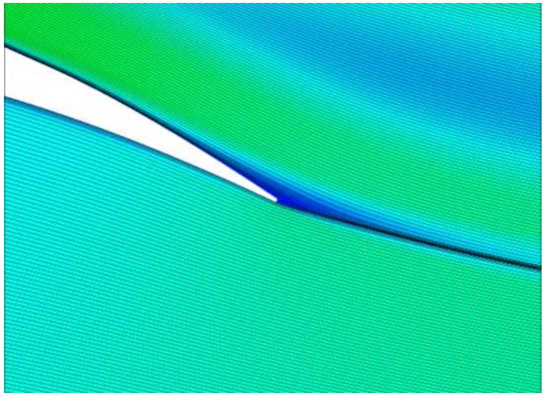

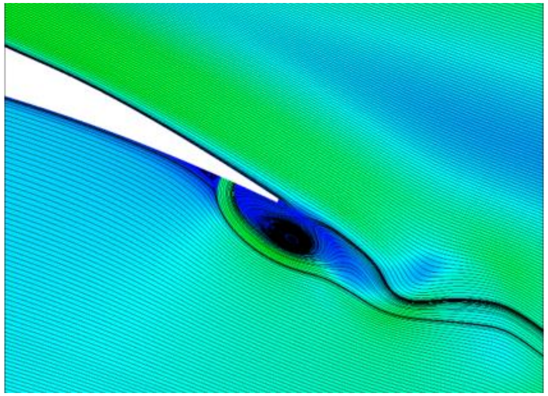

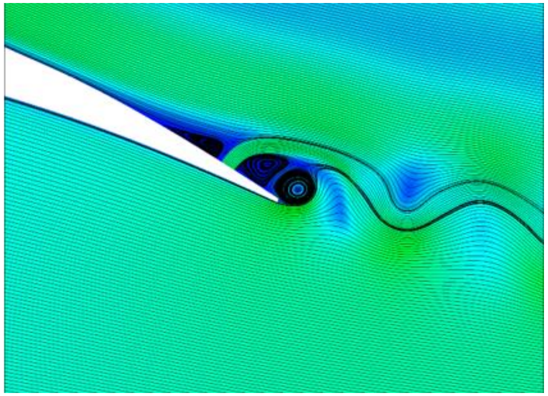

Airfoil Definition

- NLR7301: flap chord is 32%c_{ref}
  - Flap deflection 20°, overlap 0.053c, gap 0.026c
  - 2-dimentional $\alpha = 6°$, $Re = 2.51E6$, and $M = 0.185$

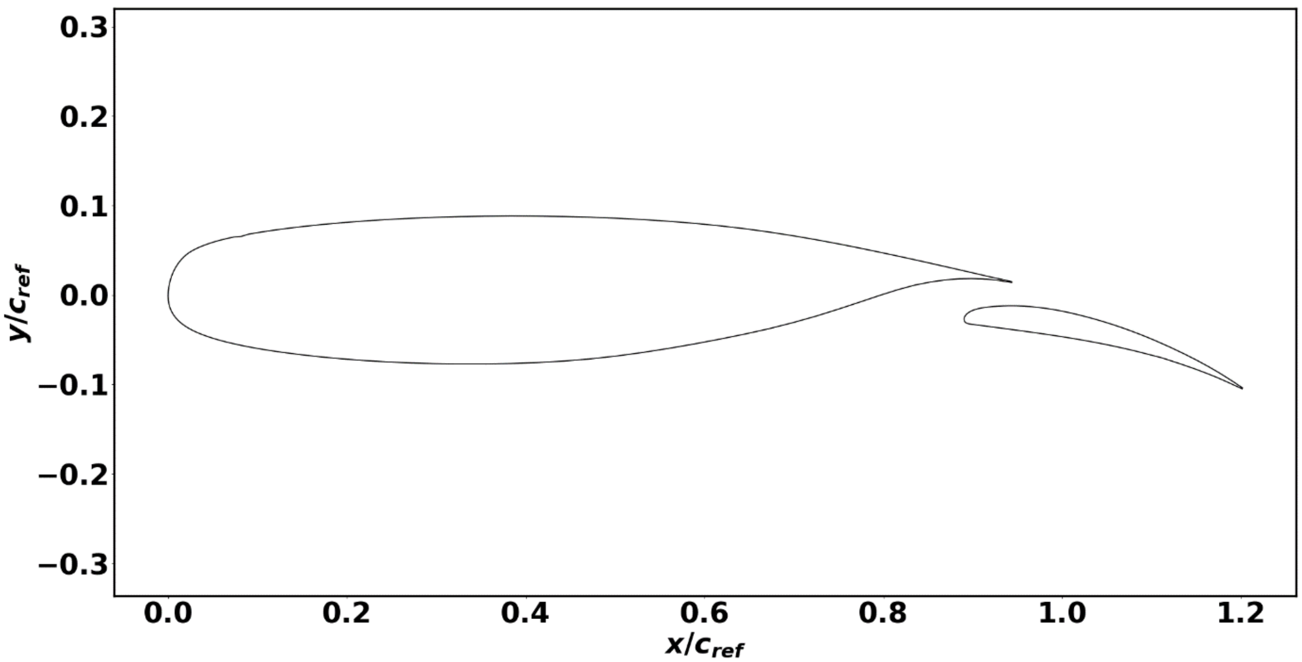

Vandenberg and Oskam 1980

2-Dimentional Computational Setup

- Overset grid technology
  - O-grid topology growing 50c away
  - DCF mesh connectivity
- RANS OVERFLOW 2
  - 4th order central difference and ARC3D diagonalized approximate factorization with matrix artificial dissipation
  - SST turbulence model

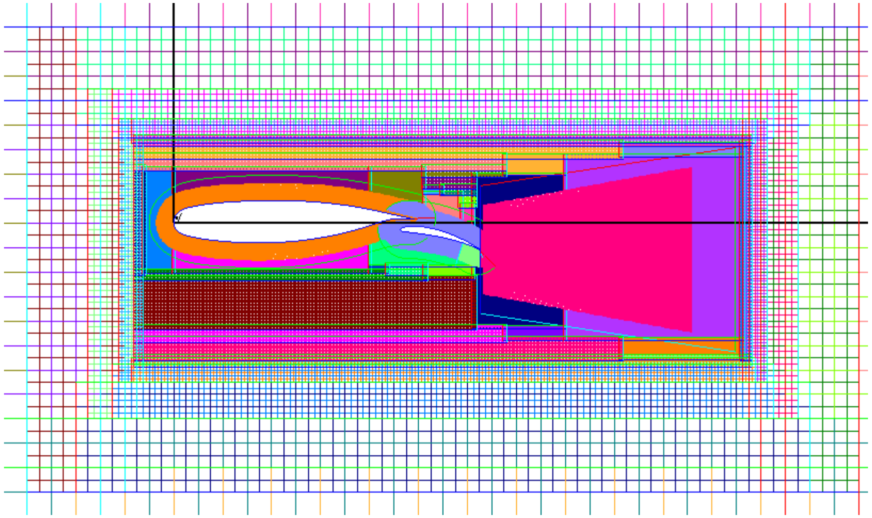

Clock Time[min] on 48 Haswell Processors	C_l	$\Delta C_l\%$ error	C_d	$\Delta C_d\%$ error
32.08	2.3946	1.05%	0.0301	31.4%

Microjet vs. Microtab Study

α=6°, Re = 2.51E6, and Ma = 0.185, Steady State

- Literature suggested 1%c in height and 0.2%c thickness tabs at 95%c
- How to model the jet?
  - Modeled as a simple jet mass flow condition at the surface
    - Suggested by: the flow control workshop held in 2004, the Blaylock dissertation
- Boundary condition $Uj/U\infty$ at flap TE was employed:

$$C\mu = \frac{\dot{m}_j U_j}{\frac{1}{2}\rho_\infty U_\infty^2 \, S_{ref}} \xrightarrow{\dot{m}_j = (\rho U A)_j} C\mu = \frac{\rho_j U_j^2 h_j b}{\frac{1}{2}\rho_\infty U_\infty^2 \, b \, c} \xrightarrow[c = 1]{Incompressible} C\mu = 2\frac{U_j^2}{U_\infty^2}\, h_j$$

Microjet vs. Microtab Study

α=6°, Re = 2.51E6, and Ma = 0.185, Steady State

	C_l	C_d
Baseline (no AFC)	2.395	
Microtab	2.626	
Microjet	2.627	

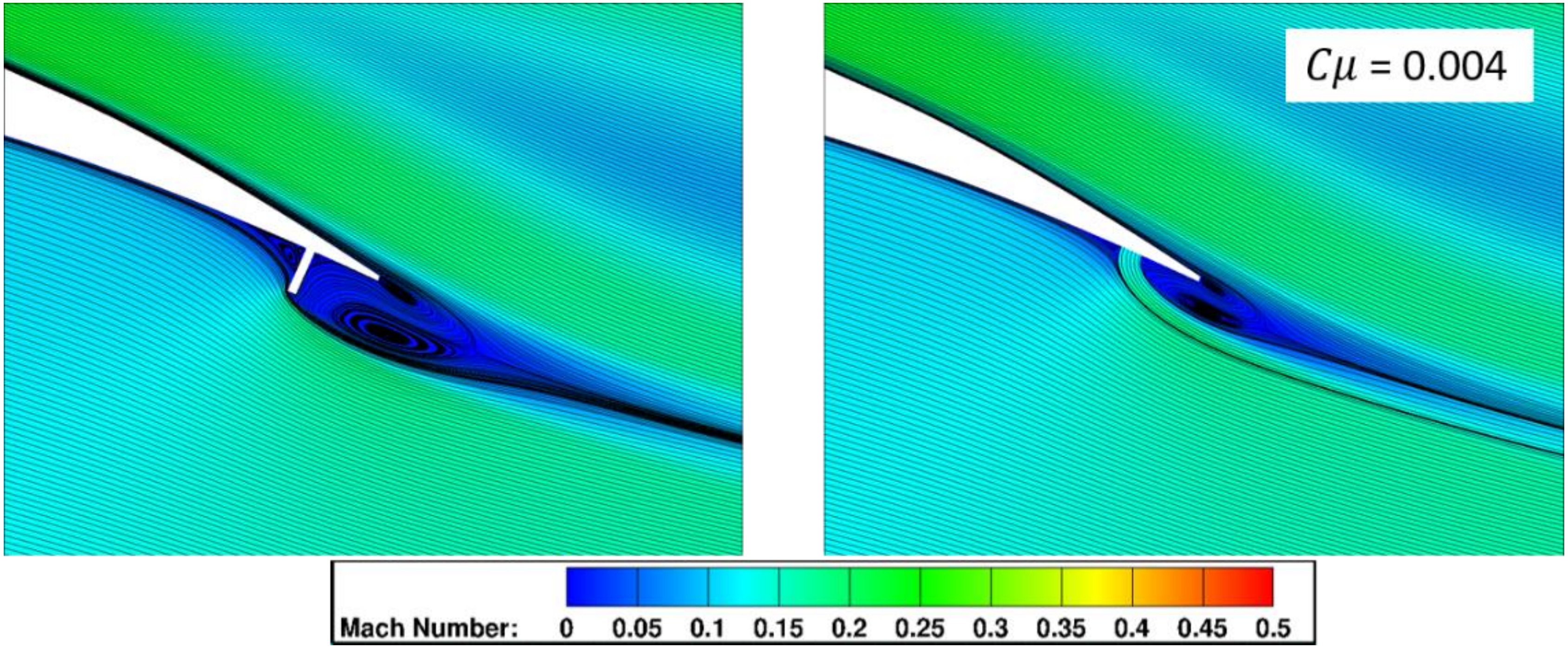

Microjet vs. Microtab Study

α=6°, Re = 2.51E6, and Ma = 0.185, Steady State

	C_l	C_d
Baseline (no AFC)	2.395	0.0301
Microtab	2.626	0.0358
Microjet	2.627	0.0284

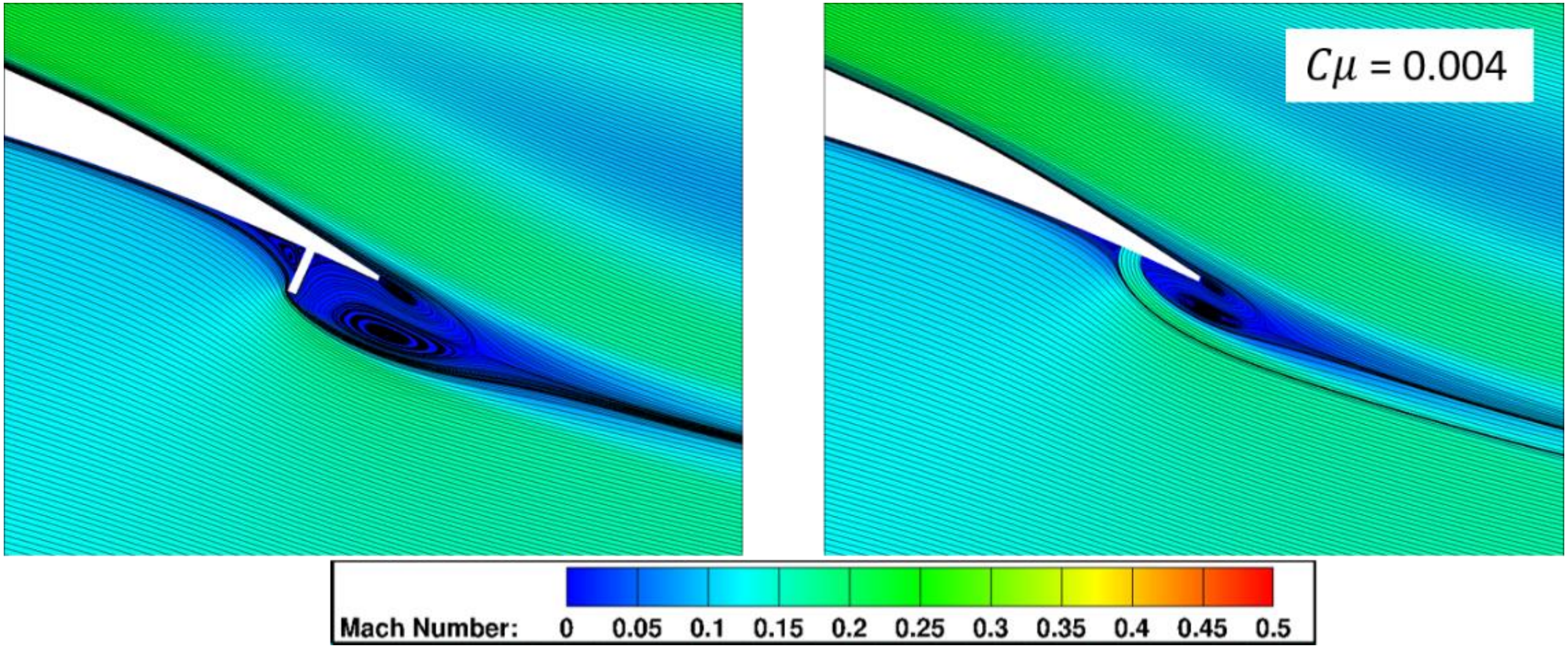

Microjet Momentum Coefficient

α=6°, Re = 2.51E6, and Ma = 0.185

- C_μ range: 0.0004-0.04 for the jet exit $h_j = 0.005$
  - $C_\mu < 0.01$ converged with steady state simulations
  - $C_\mu \geq 0.01$ required time-accurate simulations

Steps:

1. Steady state: converge the baseline airfoil (no microjet)
2. Steady state: turn on the microjet
3. If not converged, run time-accurate

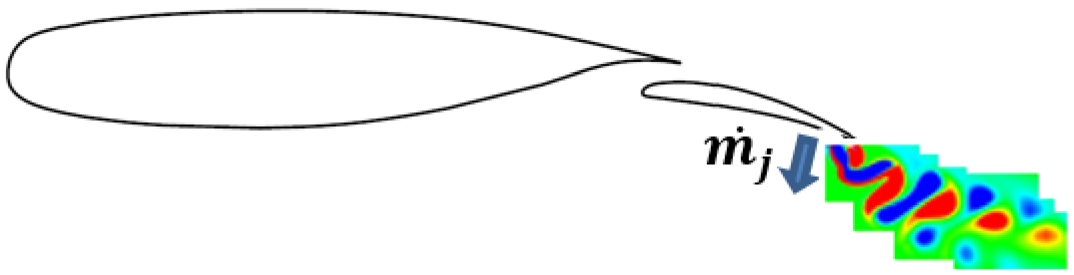

Convergence Study

α=6°, Re = 2.51E6, and Ma = 0.185, C_μ = 0.04

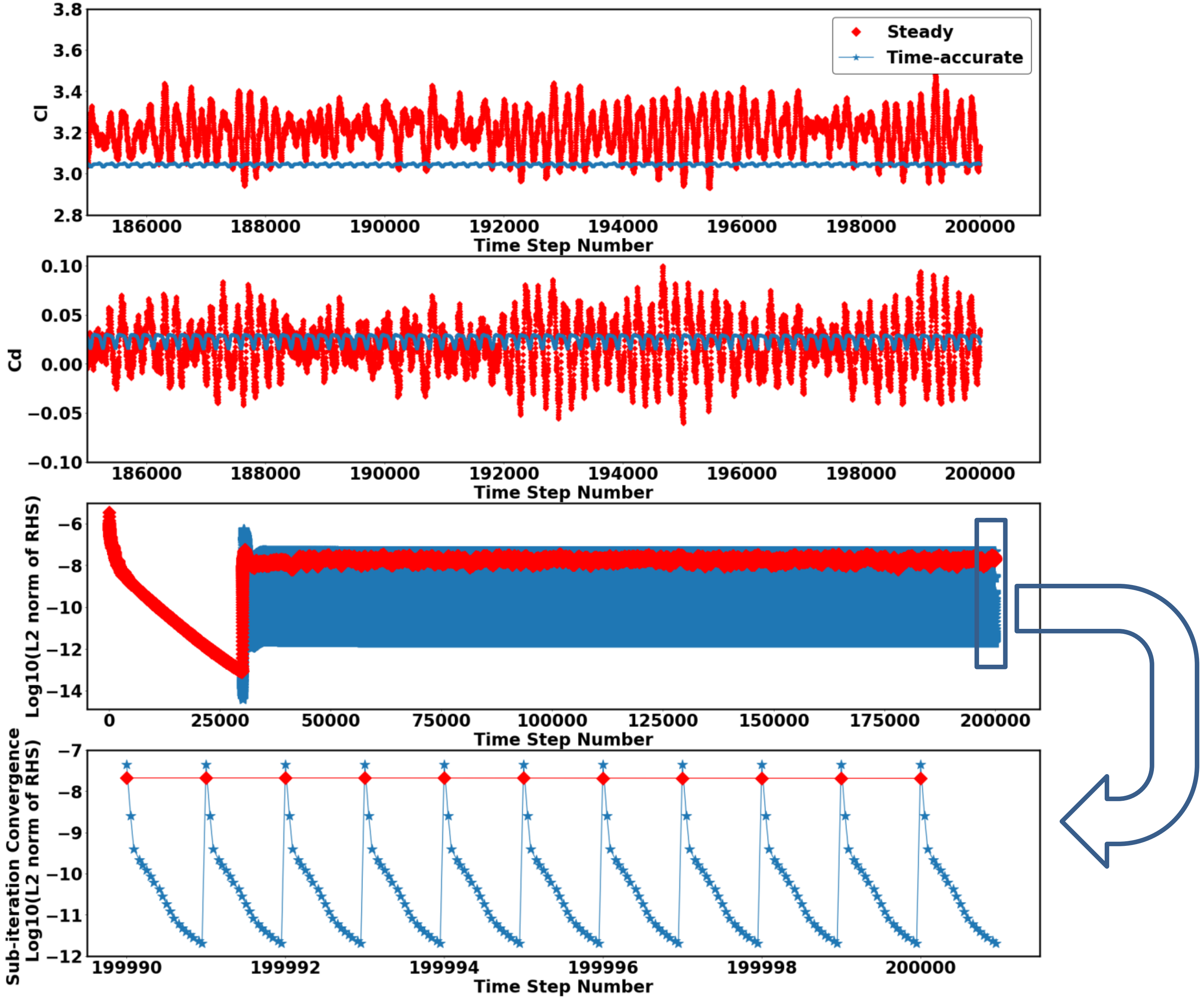

Convergence Study

α=6°, Re = 2.51E6, and Ma = 0.185, C_μ = 0.04

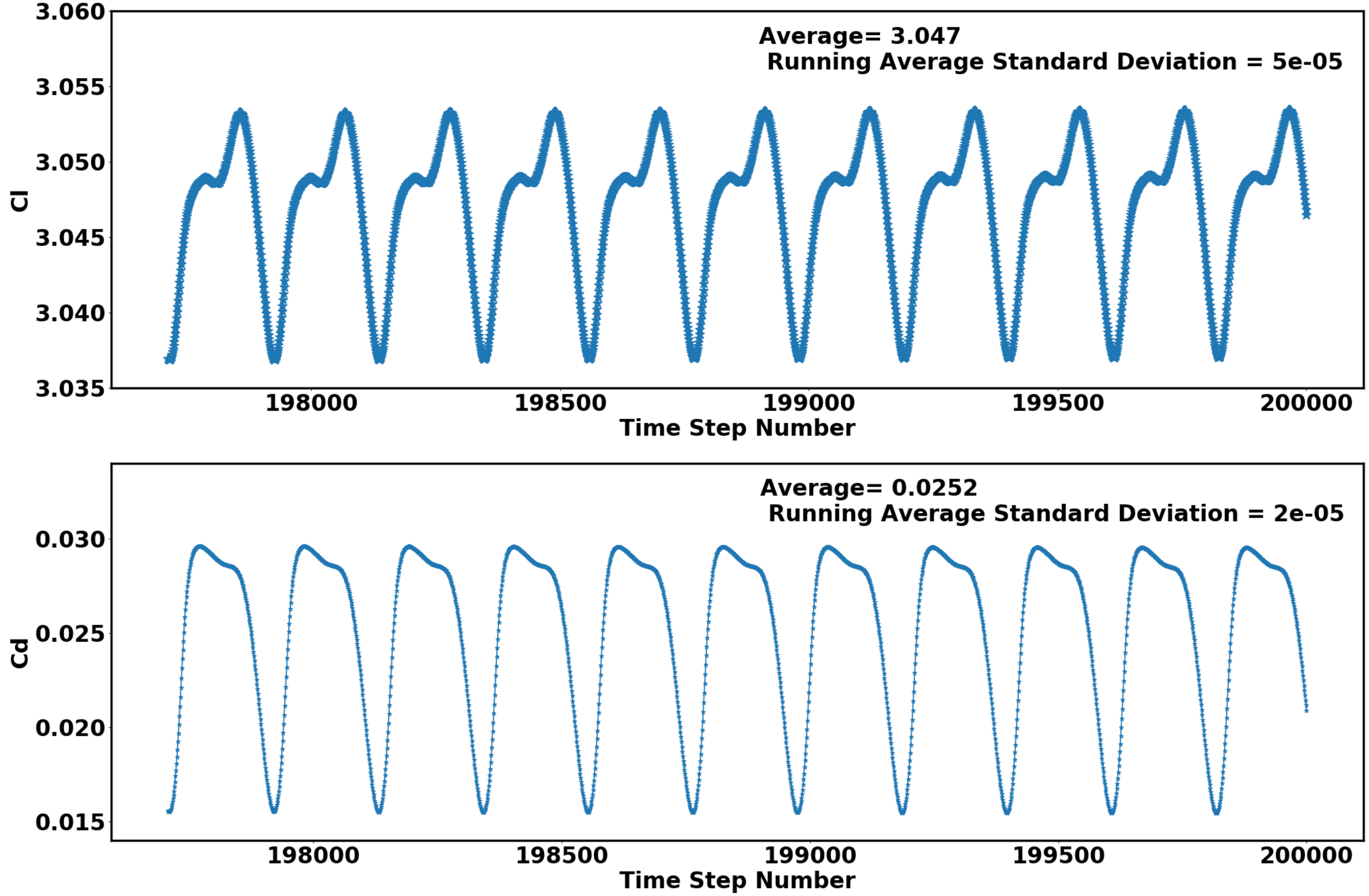

Flow Visualization

α=6°, Re = 2.51E6, and Ma = 0.185, C_μ = 0.04

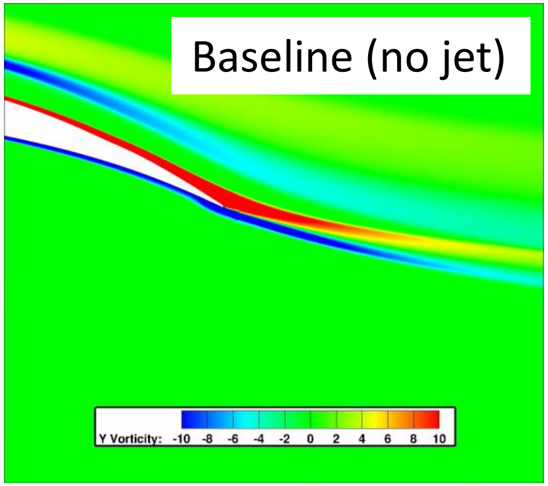

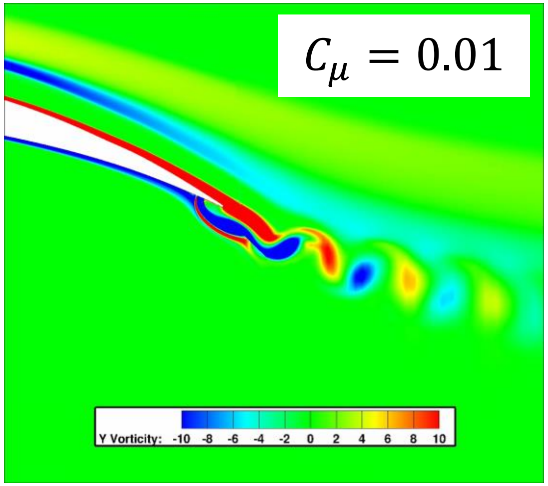

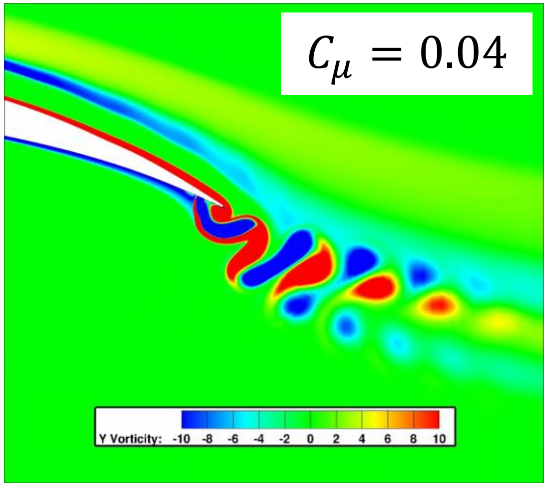

Steady

Unsteady, St = 0.072

Unsteady, St = 0.103

Momentum Coefficient Sensitivity

α=6°, Re = 2.51E6, and Ma = 0.185

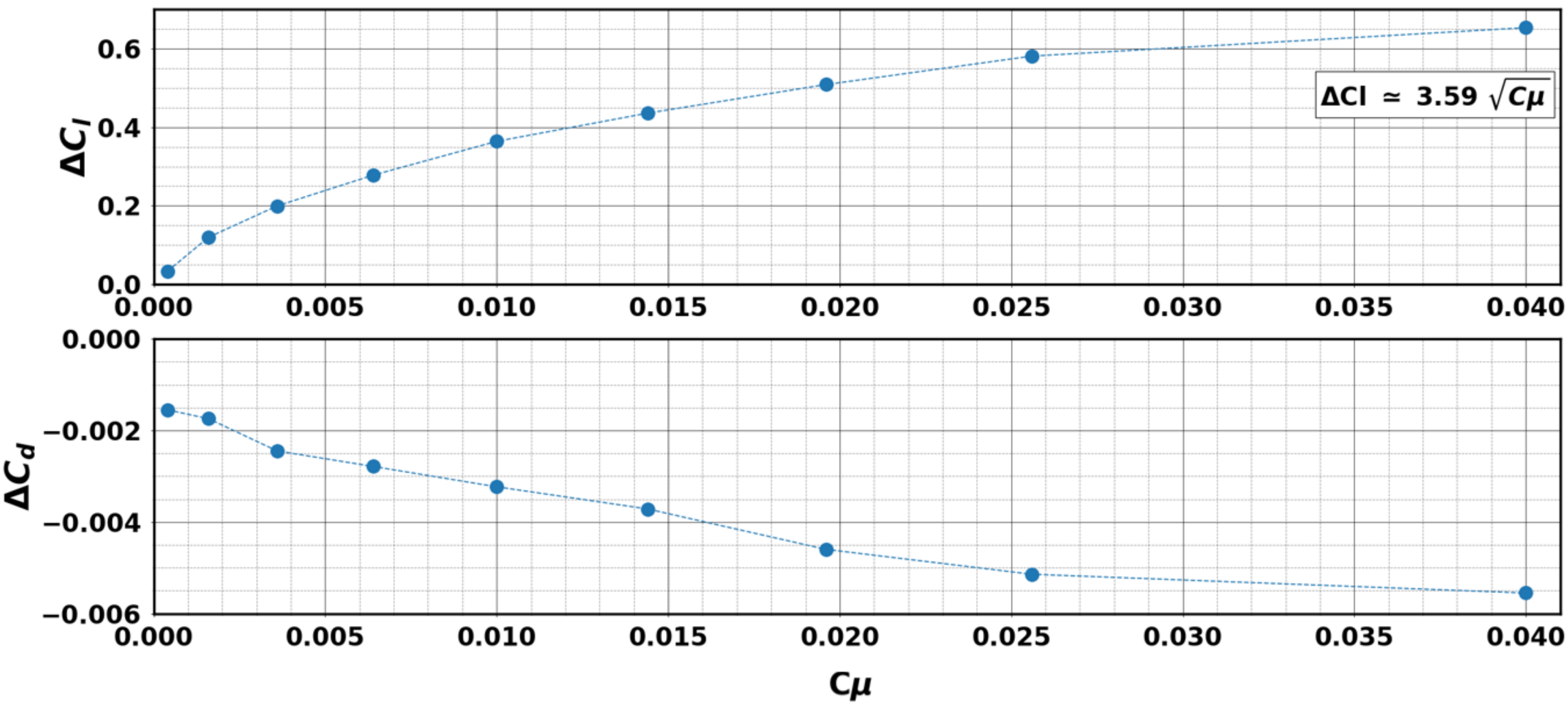

Spot Checks: Literature

Symmetric airfoil

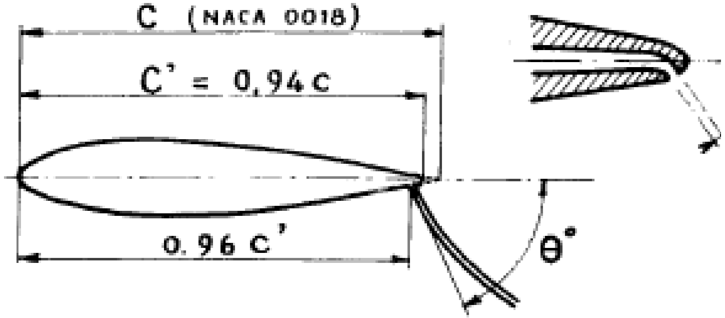

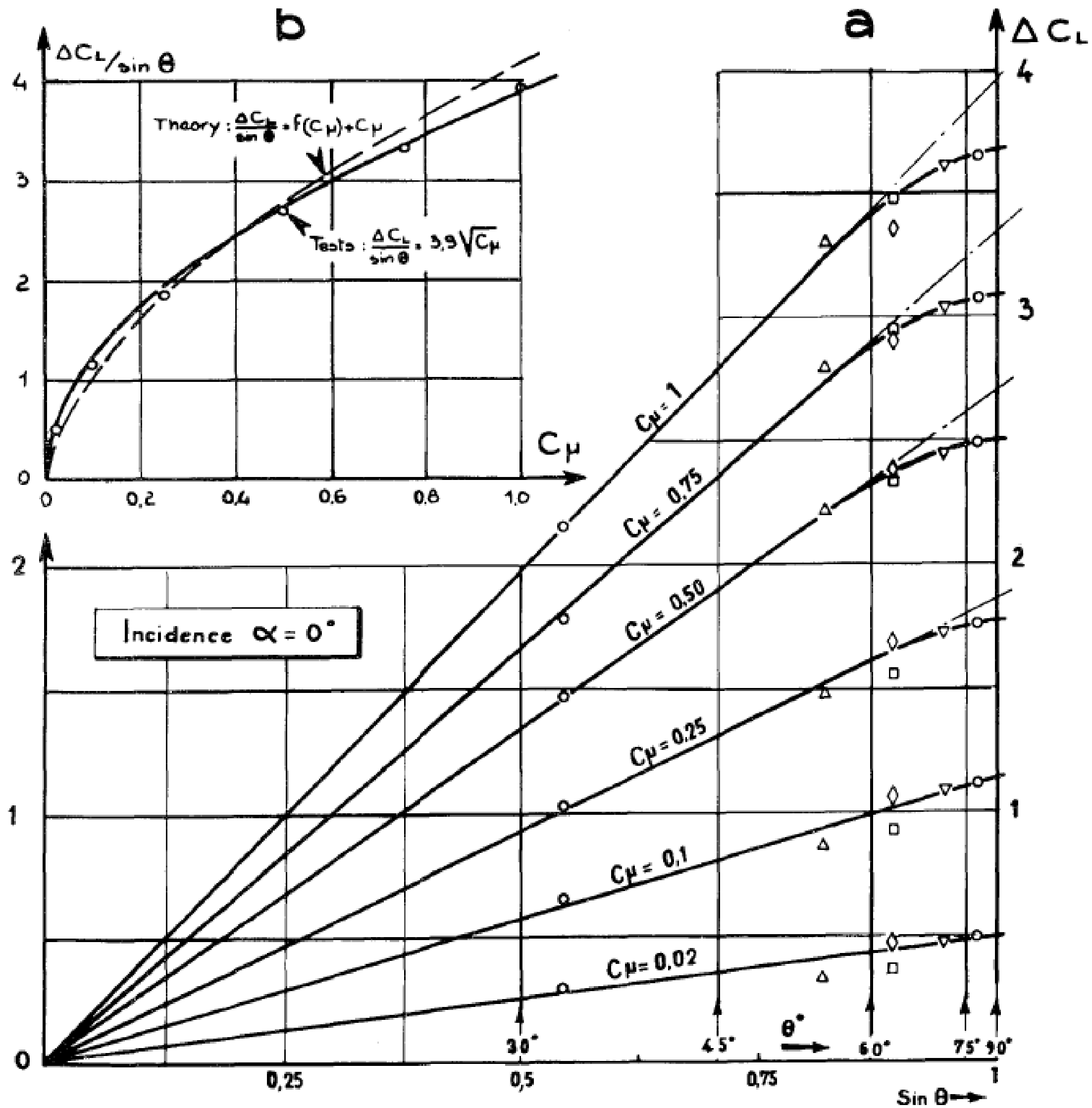

$$\Delta C_L = 3.9\sqrt{C_\mu}\cdot \sin\theta$$

Malavard 1956.

Spot Checks: Literature

Symmetric airfoil

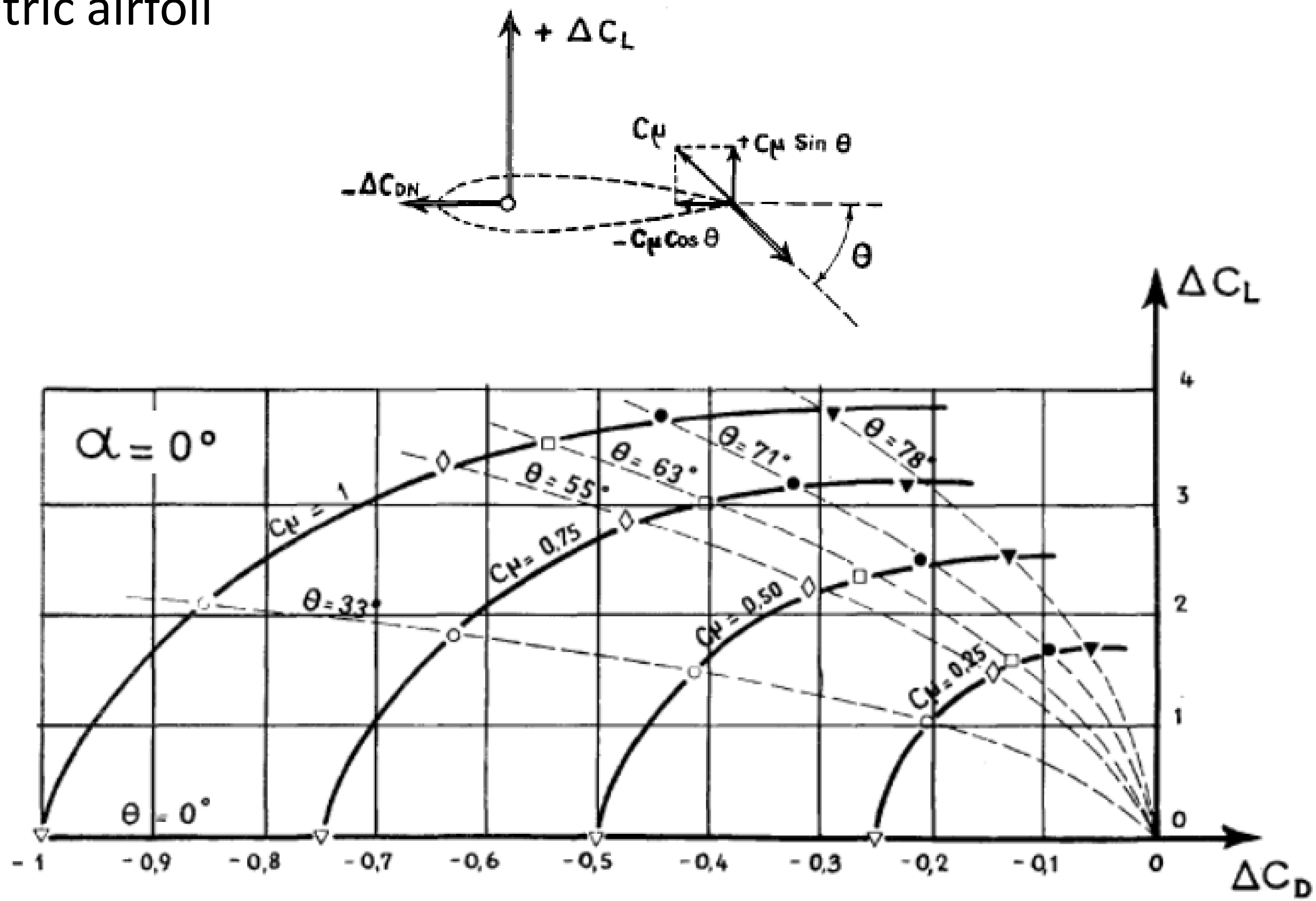

Malavard 1956.

Spot Checks: Literature

UC DAVIS COLLEGE OF ENGINEERING

Symmetric t/c = 18% airfoil

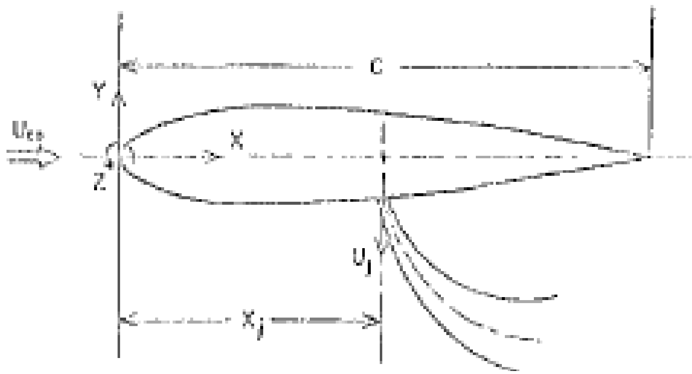

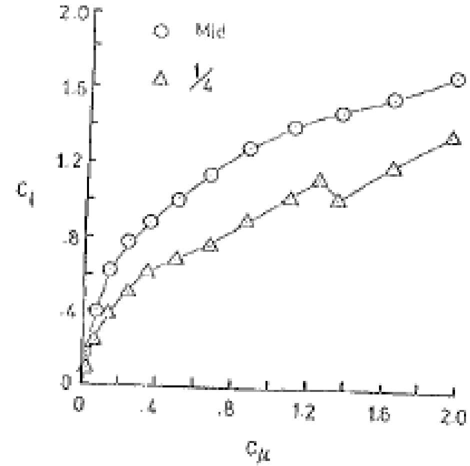

NACA 0018 airfoil

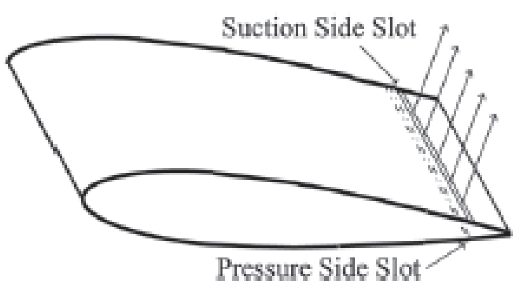

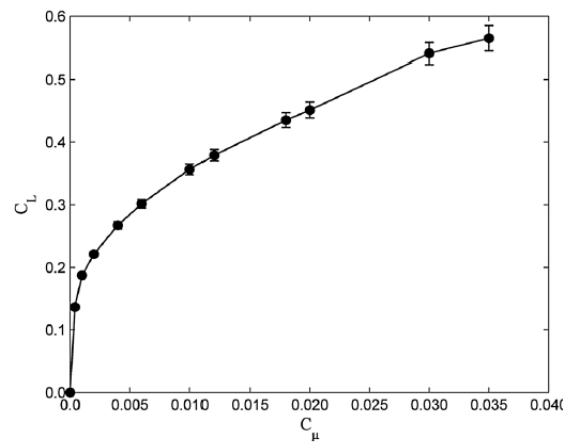

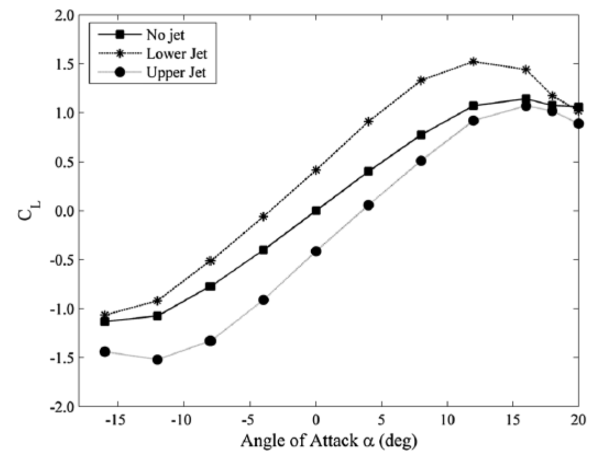

Leopold and Krothapalli 1983
Blaylock 2012

Drag Validation

α=0°, Re = 2.51E6, and Ma = 0.185, C_μ = 0.01

Case	Integration at	C_l	C_d
Baseline (no jet)	surface	1.624	0.01985
Baseline (no jet)	0.3c far-field	1.624	0.01979
Baseline (no jet)	0.5c far-field	1.624	0.01978
Baseline (no jet)	0.7c far-field	1.624	0.01977
Pressure side jet	surface	1.979	0.02285
Pressure side jet	0.3c far-field	1.980	0.02289
Pressure side jet	0.5c far-field	1.980	0.02304
Pressure side jet	0.7c far-field	1.982	0.02318

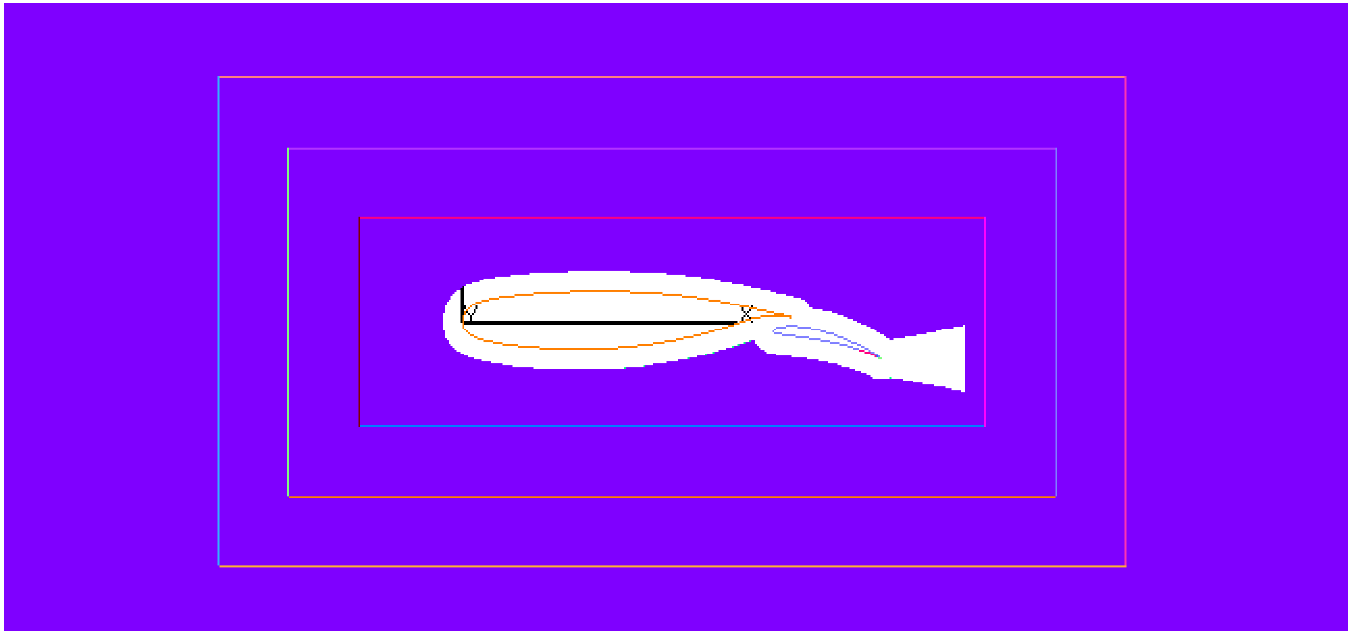

Effects on Lift and Drag

Re = 2.51E6, and Ma = 0.185, C_μ = 0.01

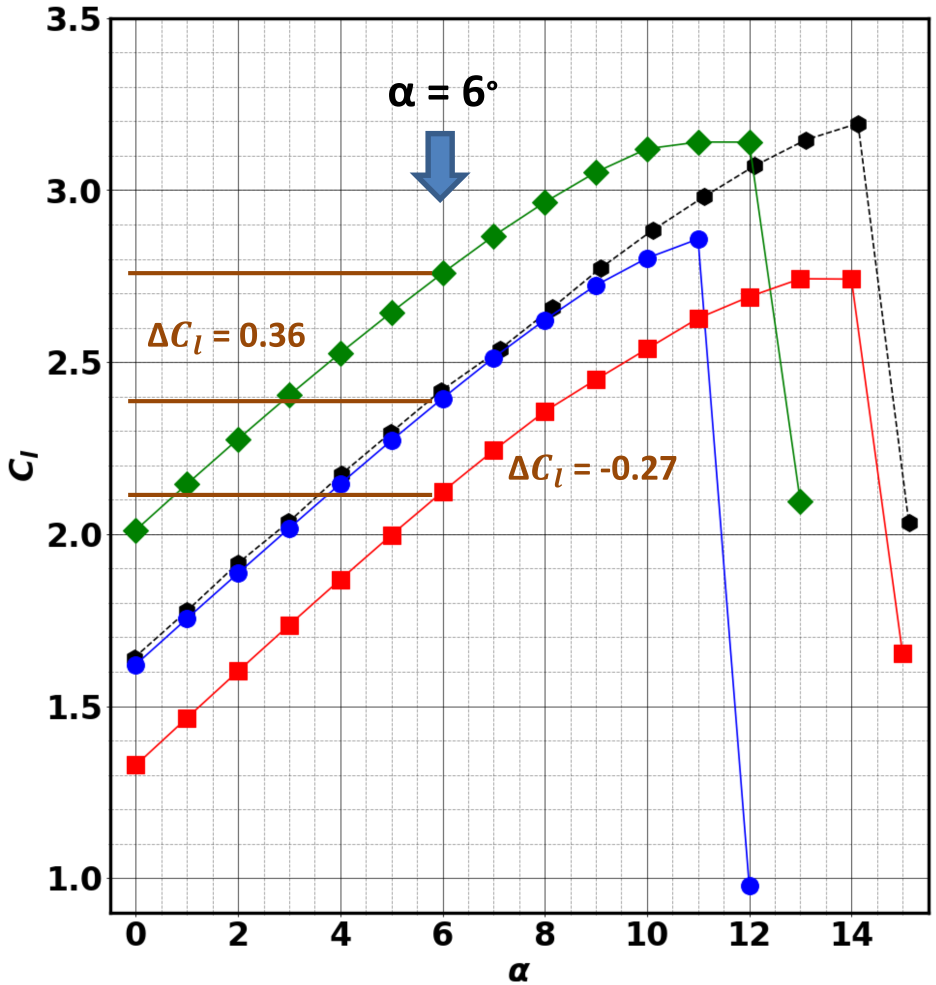

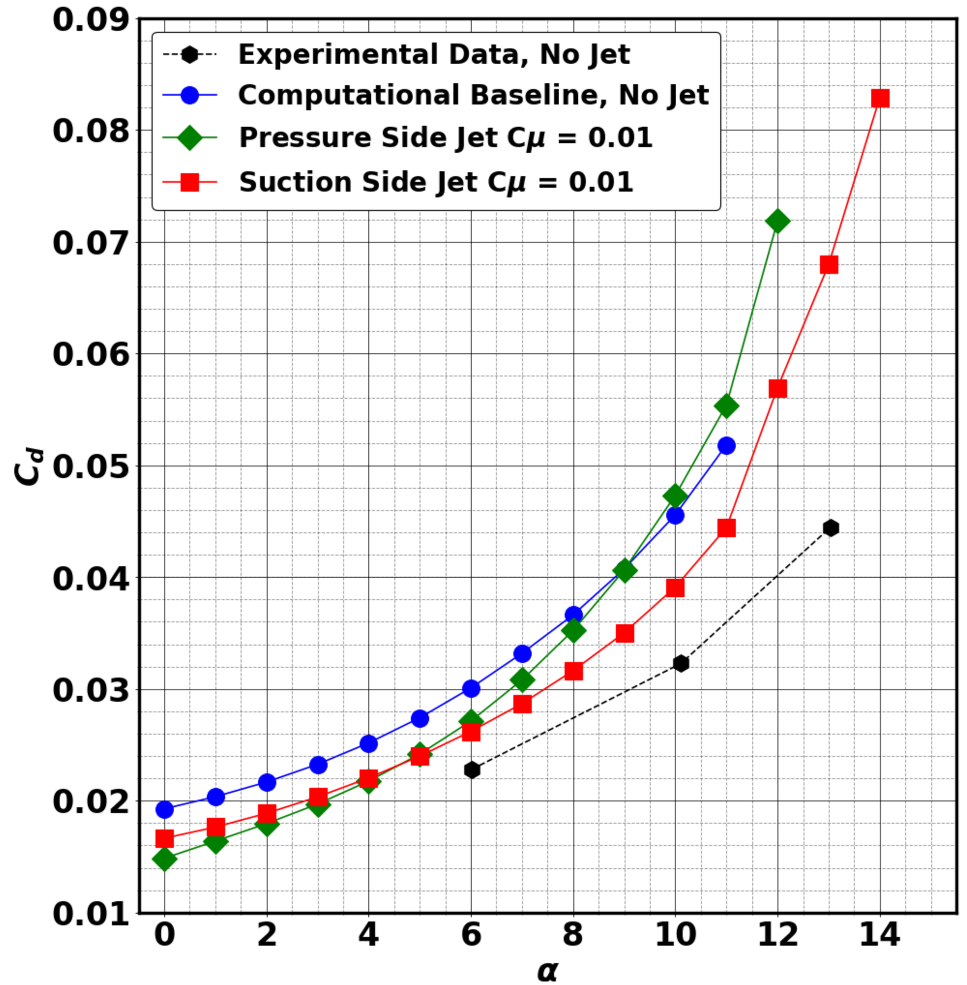

Effect on Pressure Profiles

α=6°, Re = 2.51E6, and Ma = 0.185, C_μ = 0.01

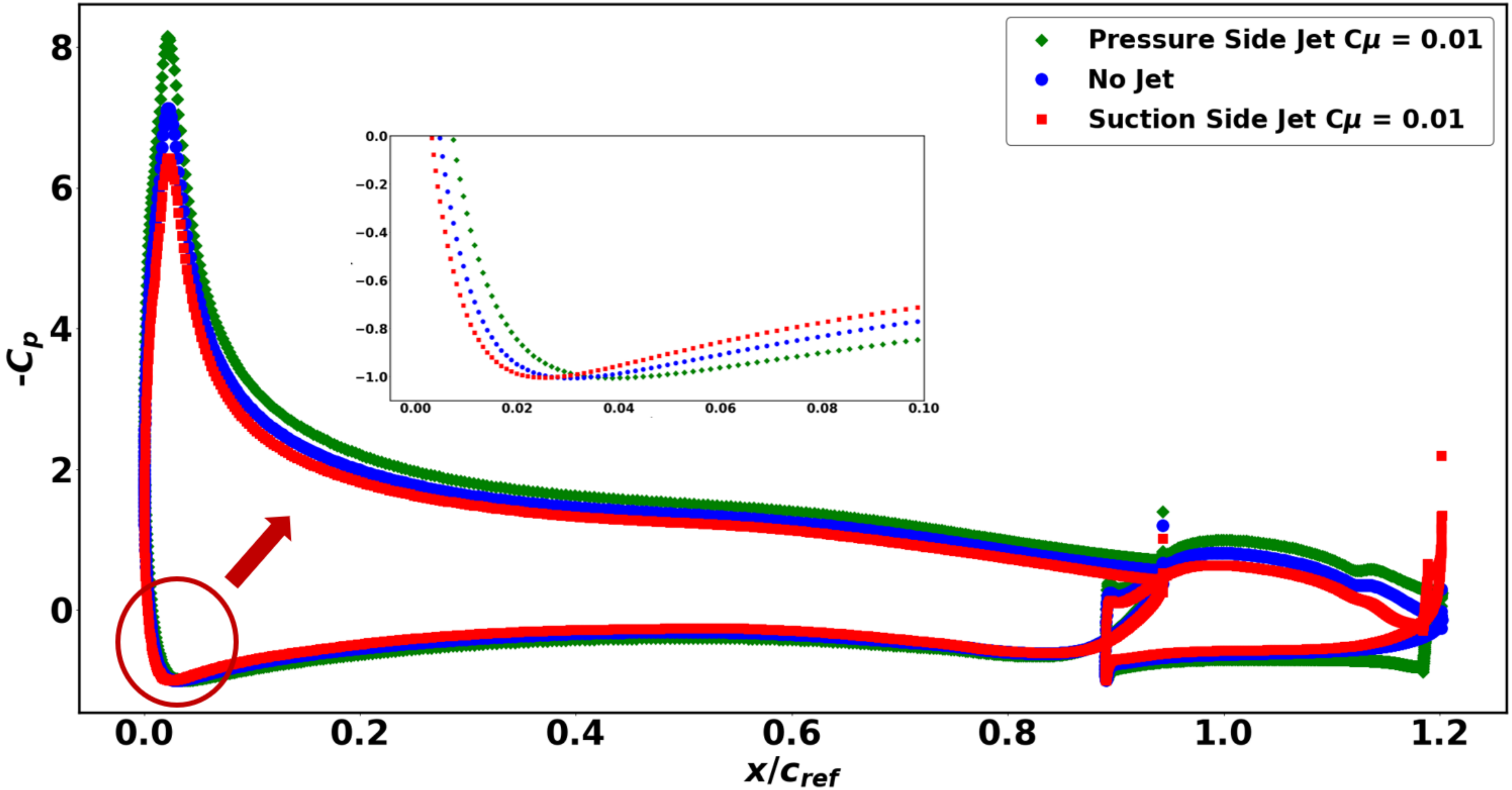

Drag Decomposition Study

Re = 2.51E6, and Ma = 0.185, C_μ = 0.01

$$\boldsymbol{F} = \int (-P\delta_{ij} + \tau_{ij})\, n_j\, dA + \int \rho u_i u_j\, n_j dA \;\Longrightarrow\; D = F_x cos\alpha + F_z sin\alpha$$

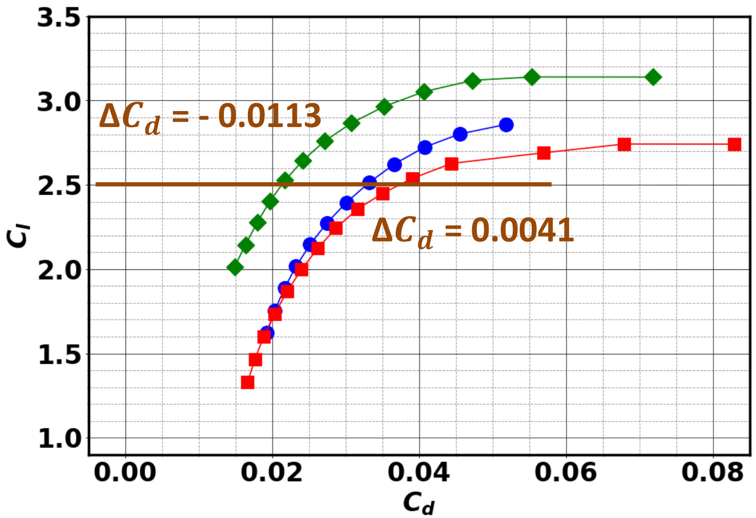

Drag Decomposition Study

Re = 2.51E6, and Ma = 0.185, C_μ = 0.01

$$\boldsymbol{F} = \int (-P\delta_{ij} + \tau_{ij})\, n_j\, dA + \int \rho u_i u_j\, n_j dA \;\Longrightarrow\; D = F_x cos\alpha + F_z sin\alpha$$

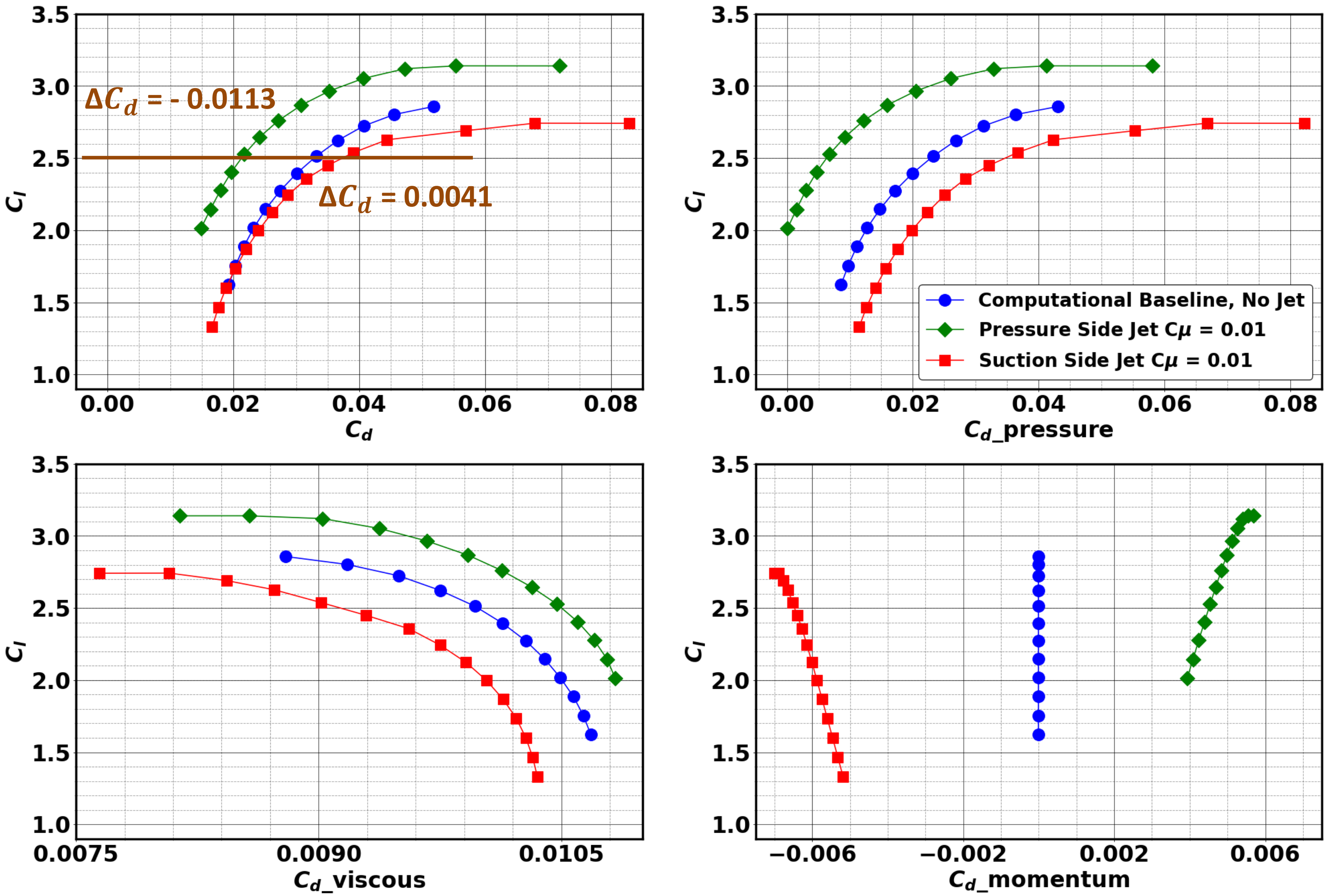

Effects on Lift and Drag

Re = 2.51E6, and Ma = 0.185, C_μ = 0.01

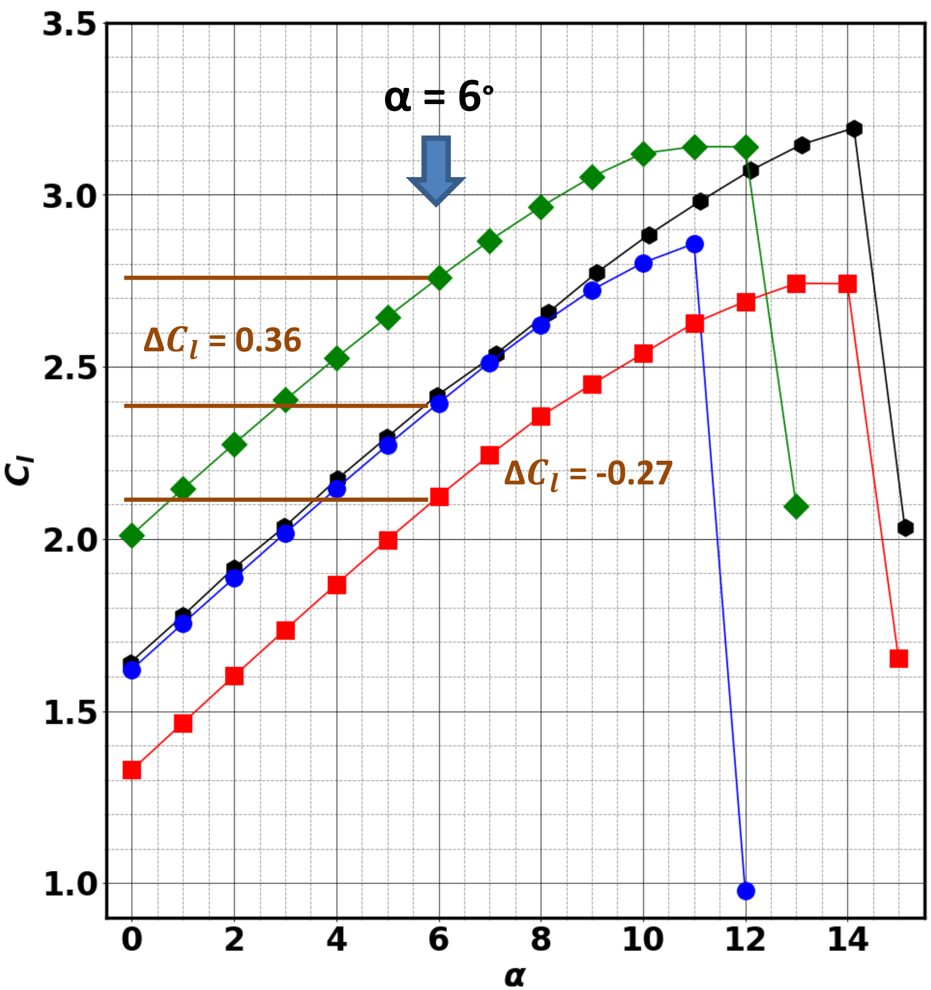

Pressure lift is 2 orders of magnitude higher than due to added momentum

C_l at α=6°	Baseline No jet	Pressure side jet	Suction side jet
Pressure	2.39414	2.75046	2.13282
Viscous	0.00048	0.00076	0.00038
Momentum	0	0.00839	-0.00760
Total	2.39466	2.75961	2.12260

$$\boldsymbol{F} = \int (-P\delta_{ij} + \tau_{ij})\, n_j\, dA + \int \rho u_i u_j\, n_j dA$$

$$L = -F_x sin\alpha + F_z cos\alpha$$

Effects on Lift and Drag

Re = 2.51E6, and Ma = 0.185, C_μ = 0.01

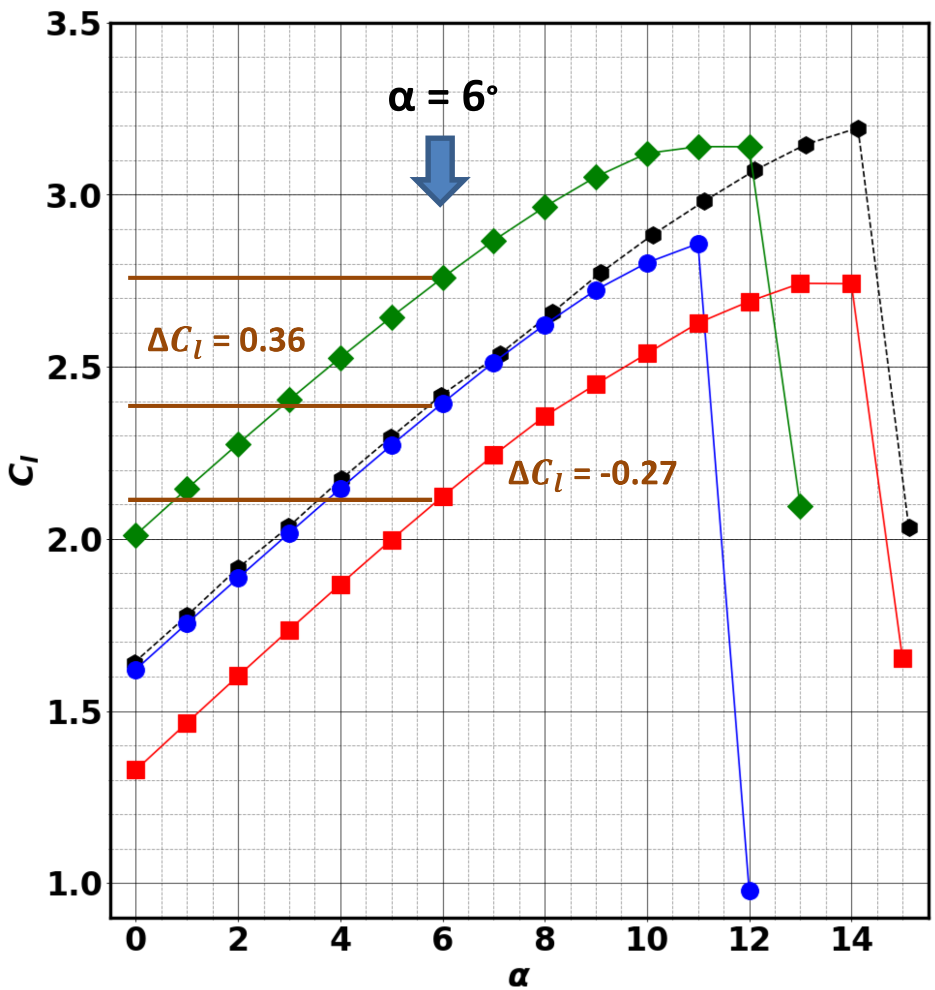

Pressure lift is 2 orders of magnitude higher than due to added momentum

C_l at α=6°	Baseline No jet	Pressure side jet	Suction side jet
Pressure	2.39414	+0.35632	-0.26132
Viscous	0.00048	+0.00028	-0.00010
Momentum	0	+0.00839	-0.00760
Total	2.39466	2.75961	2.12260

$$\boldsymbol{F} = \int (-P\delta_{ij} + \tau_{ij})\, n_j\, dA + \int \rho u_i u_j\, n_j dA$$

$$L = -F_x sin\alpha + F_z cos\alpha$$

Microjet vs. Microtab: Drag

α=6°, Re = 2.51E6, and Ma = 0.185, Steady State

C_d at α=6°	Baseline No jet	Pressure side tab	Pressure side jet
Pressure	0.01995	0.02576	0.01622
Viscous	0.01014	0.01006	0.01007
Momentum	0	0	0.00211
Total	0.03008	0.03582	0.02839

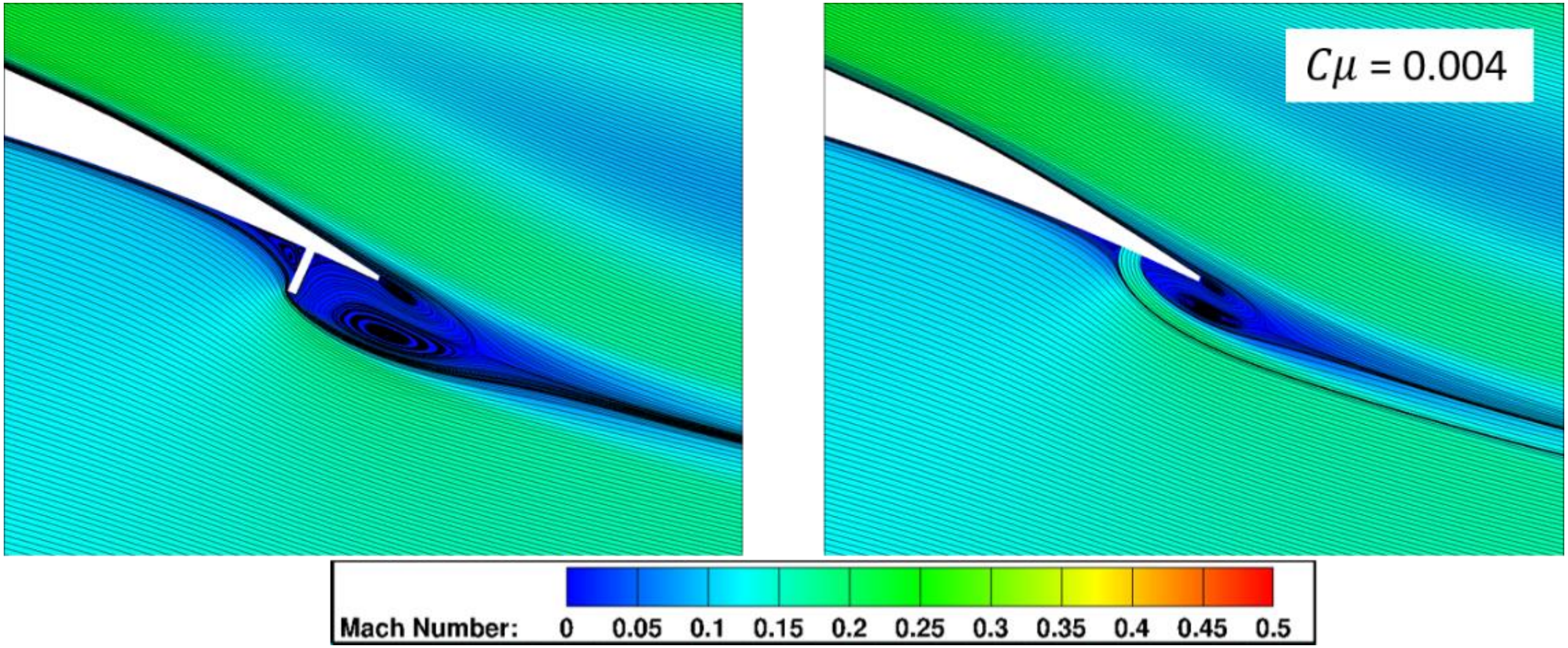

Conclusion

- The high lift system is a critical component of transport airplanes. E.g., for a large twin-engine civil transport jet on takeoff/landing (Boeing, 1993):
  - Δ(L/D) = +1% results in an increase in airplane payload of 2,800 lb assuming second-segment climb limited performance
  - $\Delta C_{L_{max}}$ = +1.5% results in an increase in airplane payload of 6,600 lb at fixed approach speed
  - ΔC_L = +0.10 reduces required landing gear height results in a reduction in airplane empty weight of 1,400 lb
- This study focuses on the application of AFC for airplane high lift systems
  - Involves a nominally-orthogonal jet injecting momentum normal to the airfoil surface near the flap trailing edge, where it modifies the trailing edge flow and, thereby, the airfoil circulation.
- The initial 2-D CFD results for the two-element high lift airfoil demonstrate the feasibility of the microjet concept for high lift system performance enhancement and aerodynamic load control.
  - Ability to shift lift curve up (blowing on pressure side of flap) and down (blowing on suction side of flap) in linear regime of the curve
  - Modify the stall angle and maximum lift coefficient of the multi-element airfoil
  - Improve lift-to-drag ratio of the multi-element airfoil

Acknowledgment

The research reported in this paper was partially funded by Boeing Commercial Airplanes (BCA), The Boeing Company. The computing resources were provided by the NASA Ames Research Center (ARC). ATTEE??? The authors acknowledge the help and inputs by Dr. Paul Vijgen, BCA, and Dr. William Chan and Dr. H. Dogus Akaydin, NASA ARC.

Immediate Next Steps

- Complete the microjet feasibility study on the two-element NLR7301 airfoil
- Validate CFD jet behavior:
  - Malavard et al (1956) experimental results
- 3-D Reynolds-averaged Navier-Stokes on NLR7301 flapped airfoil (or other multi-element airfoil configuration). Various microjet configurations

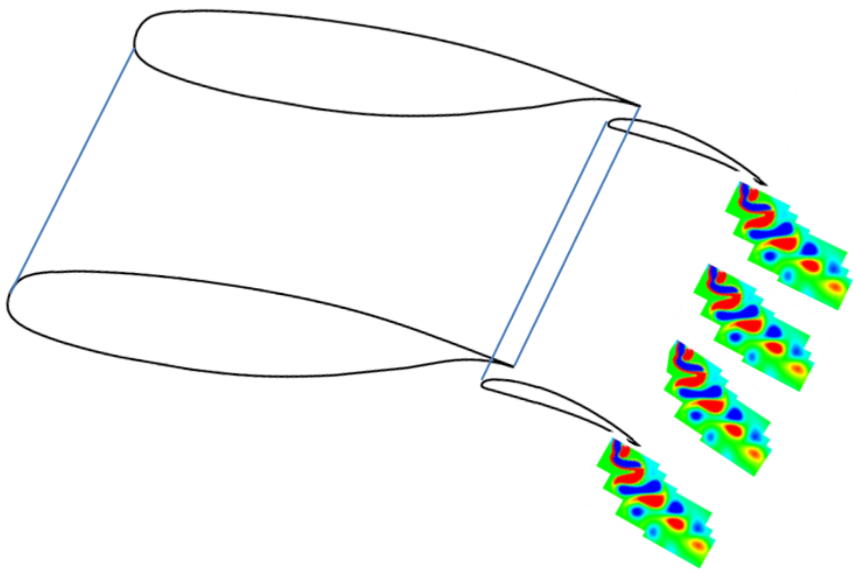

Thank you

BACKUP

Computational Setup/Validation

- Overset grid technology
  - O-grid topology growing 50c away
  - PEGASUS mesh connectivity
- RANS OVERFLOW 2
  - 4th order central difference and ARC3D diagonalized approximate factorization with matrix artificial dissipation
  - SA turbulence model

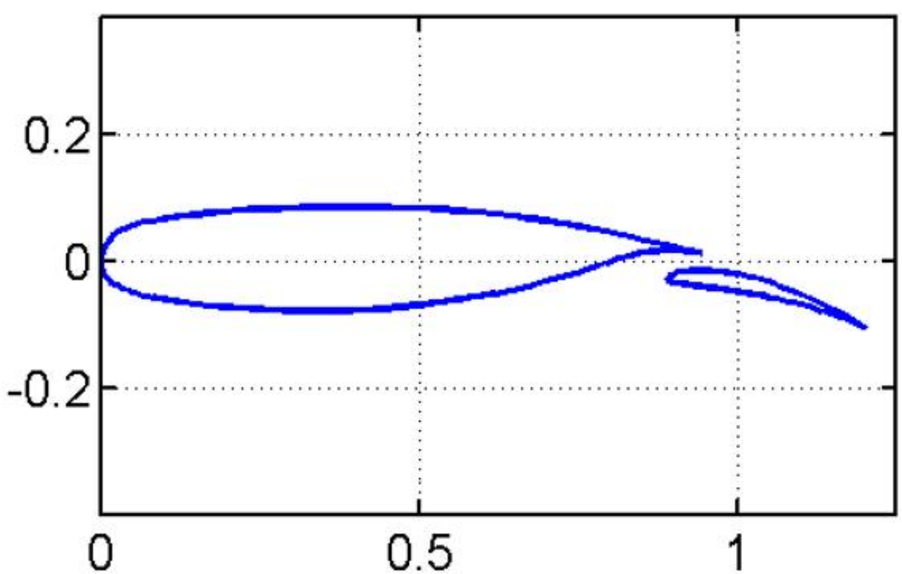

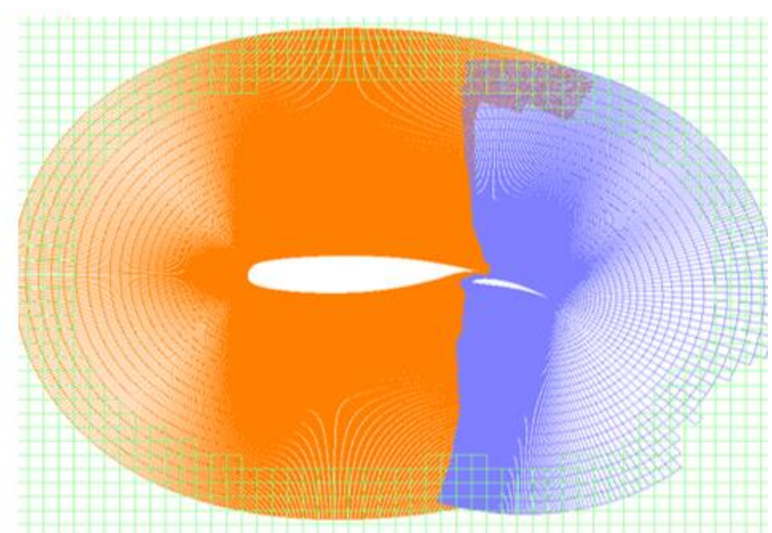

NLR7301 Experimental Data

- Reported accuracy
  - C_l within ±0.4%
  - C_d within ±2%
  - C_p within ±0.5%
  - α within ±0.05 °

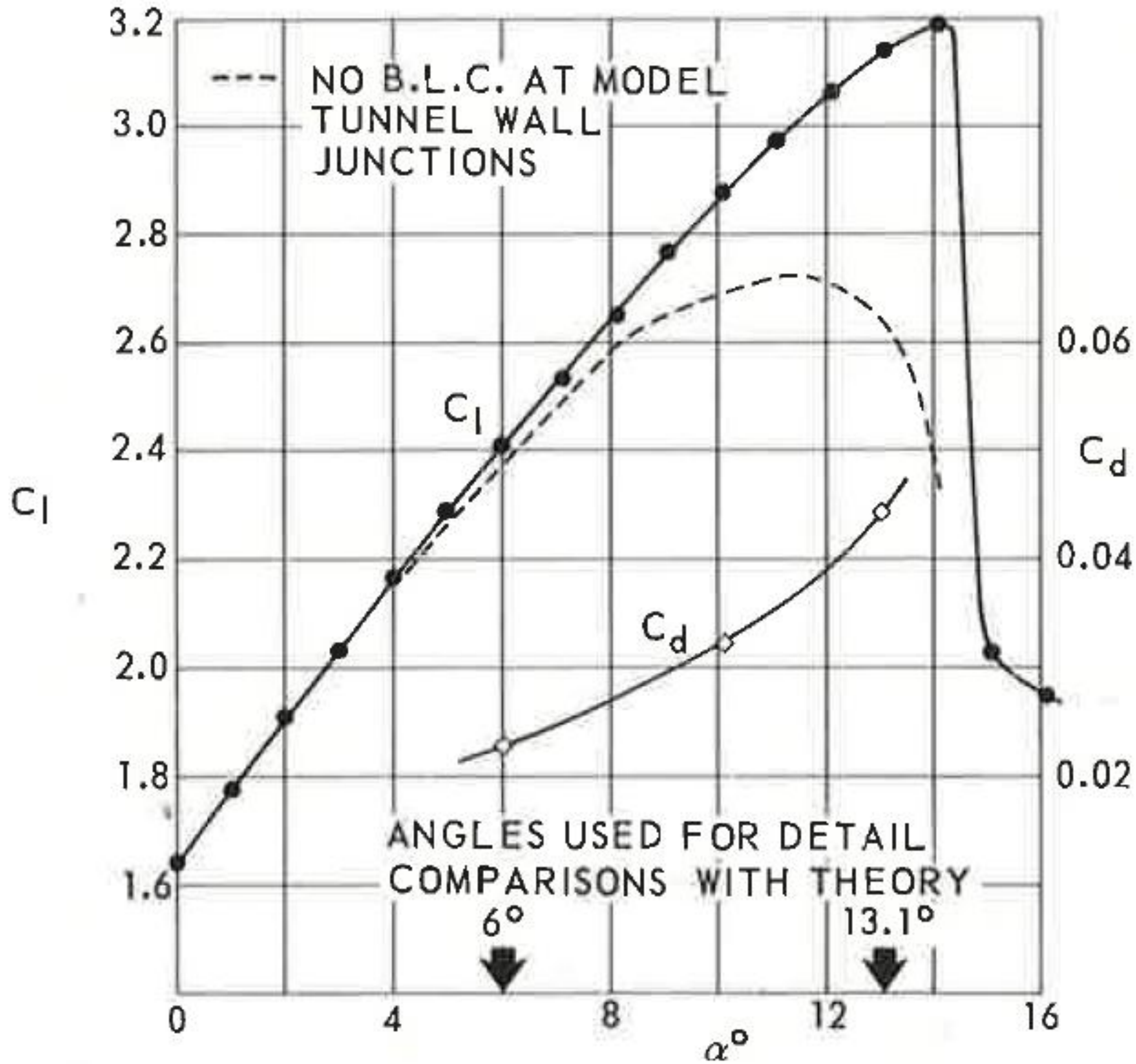

Vandenberg and Oskam 1980

NLR7301 Experimental Data

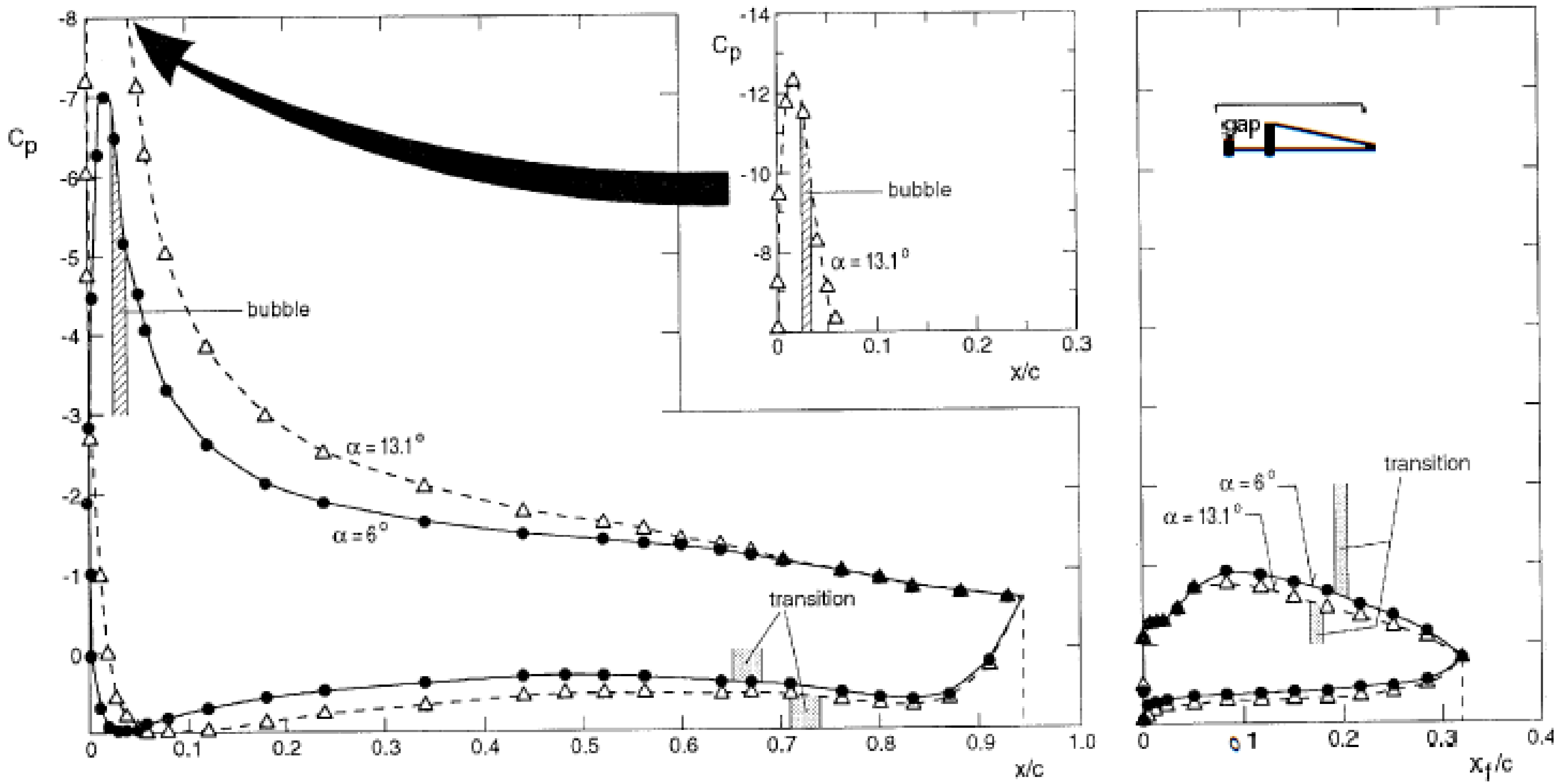

Vandenberg and Oskam 1980

Surface Grid Sensitivity

α=6°, Re = 2.51E6, and Ma = 0.185, Steady State

	Main Element	Flap Element
Coarse	600	300
Medium	800	400
Fine	1000	500
Extra-fine	1200	600

Main TE thickness: 0.0009

Flap TE thickness: 0.00115

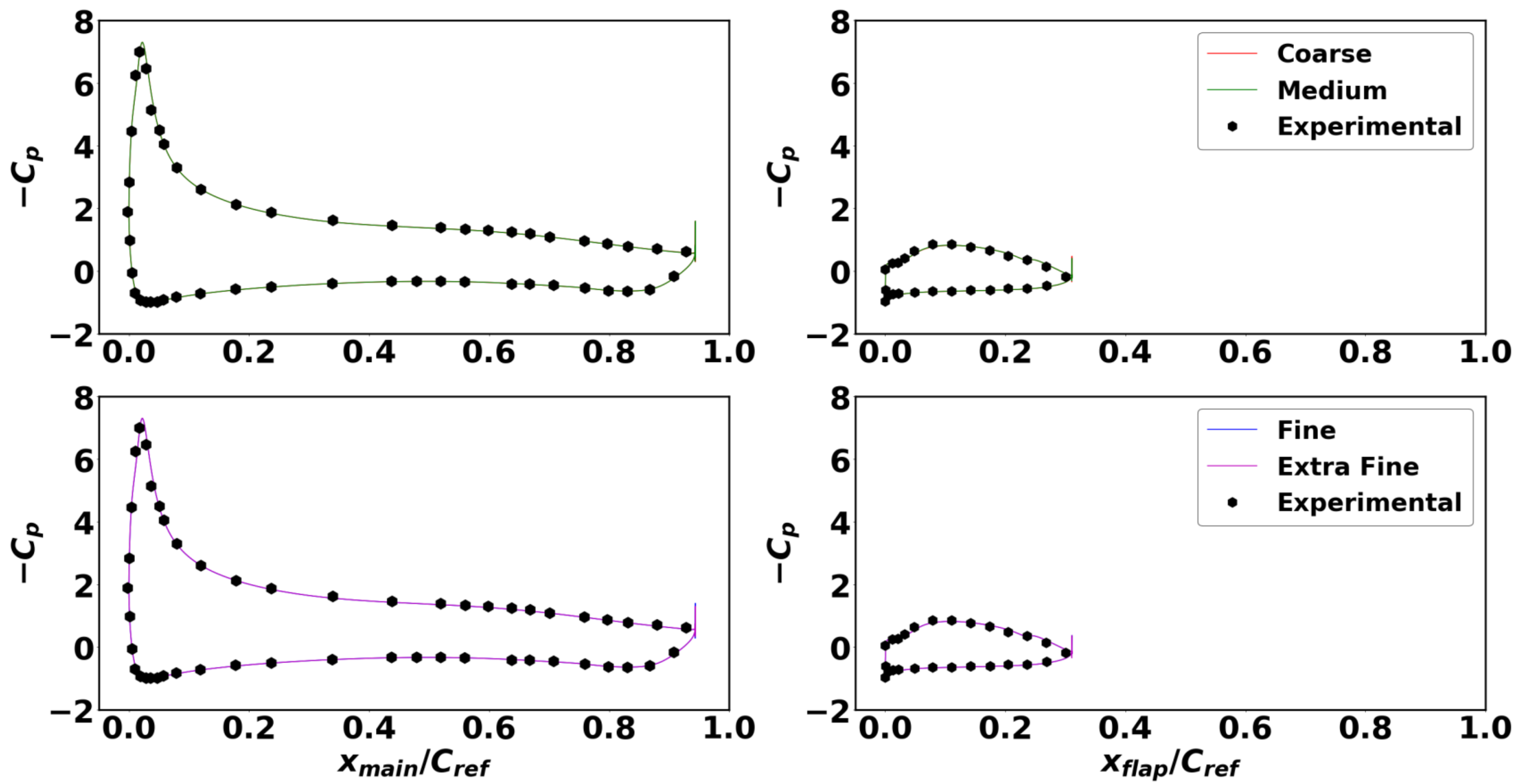

Surface Grid Sensitivity

α=6°, Re = 2.51E6, and Ma = 0.185, Steady State

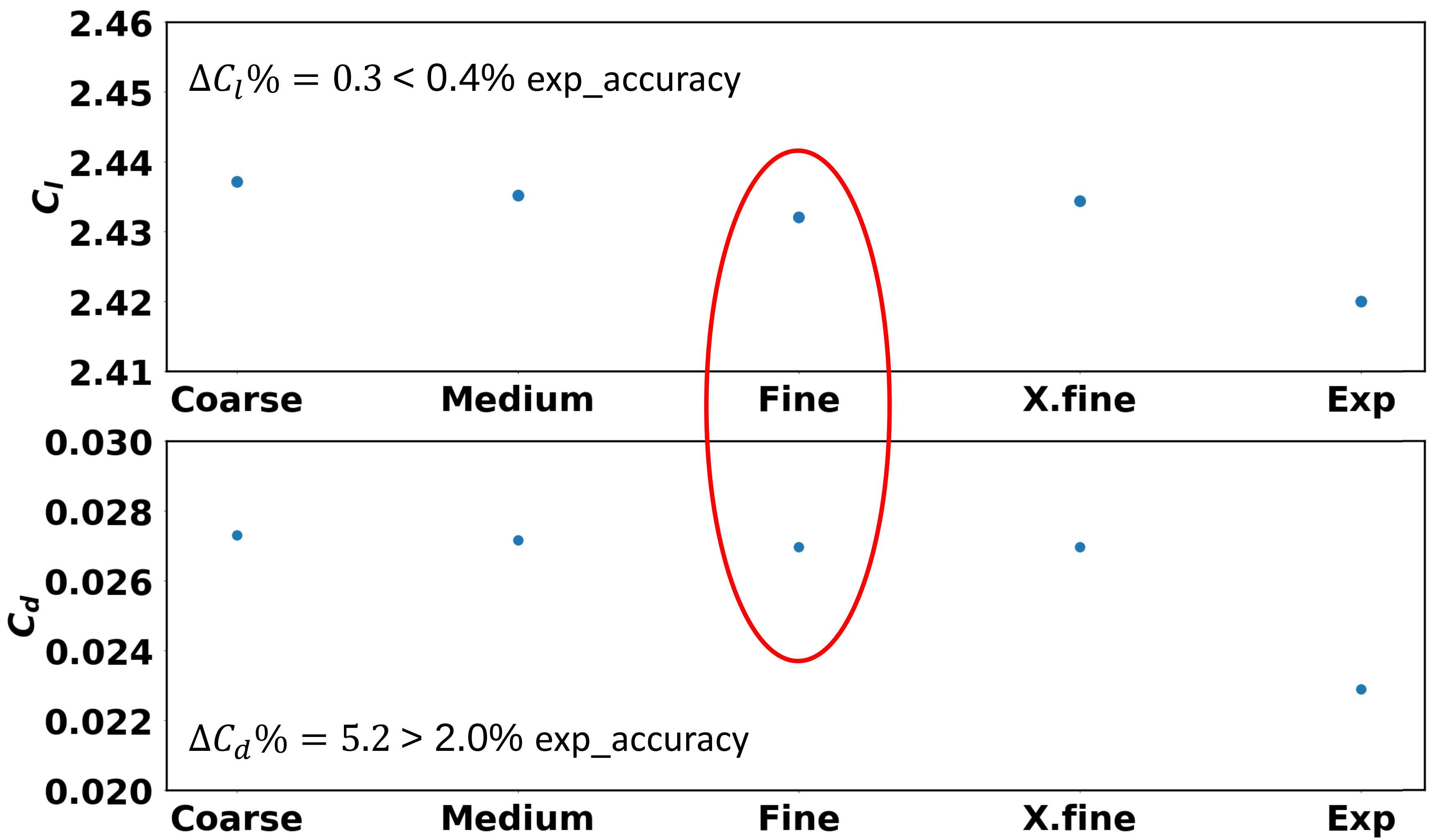

Volume Grid Refinement

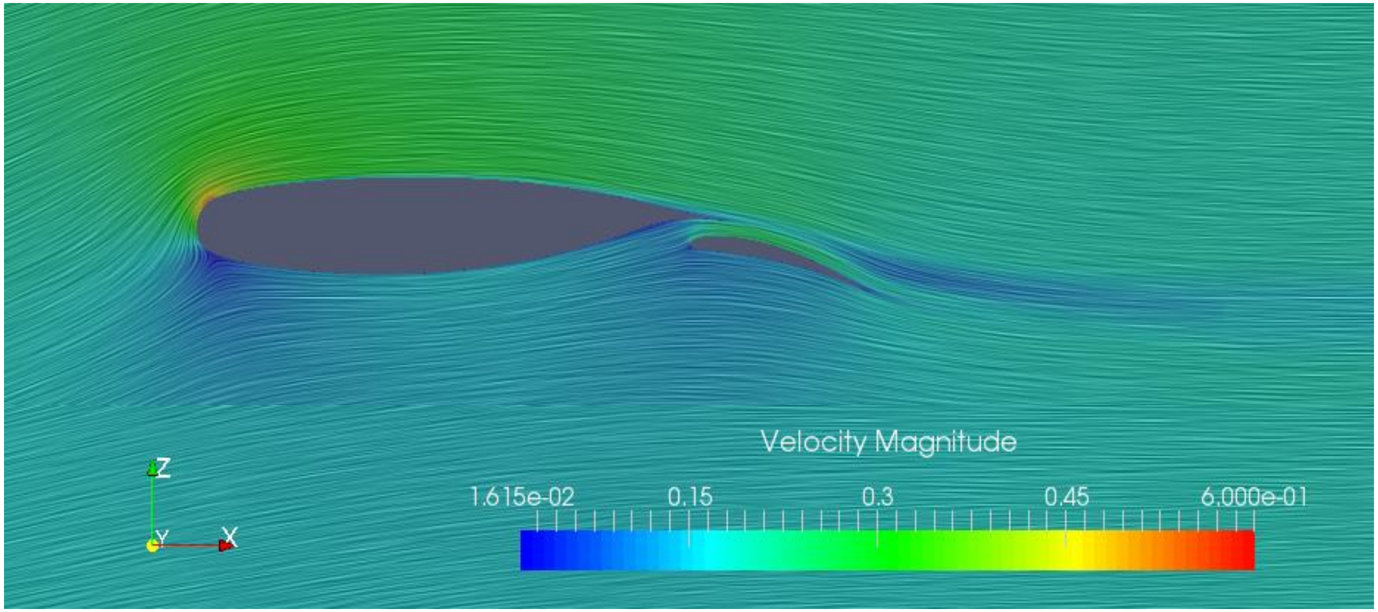

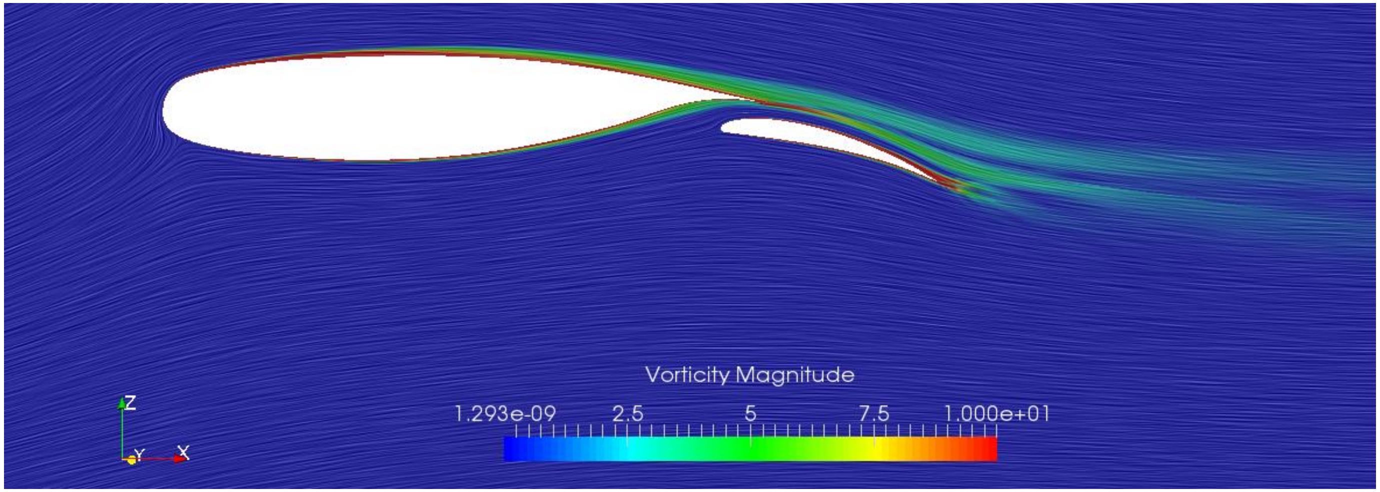

Volume Grid Sensitivity

α=6°, Re = 2.51E6, and Ma = 0.185, Steady State

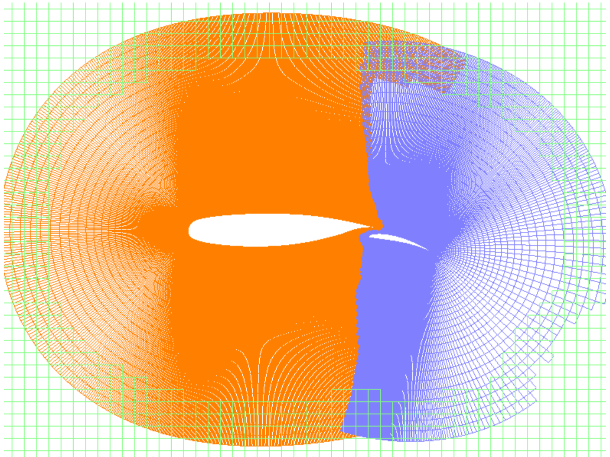

Flap grid refinement to capture the shear layer leaving the main element TE

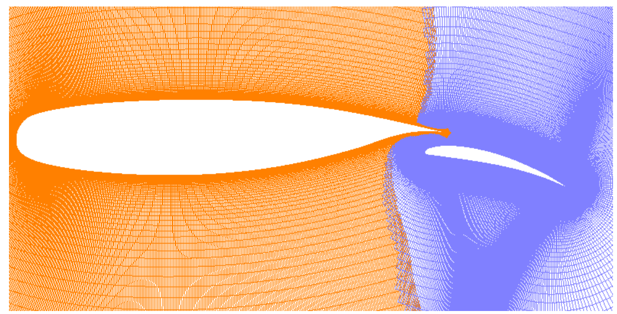

Wake grid addition to capture flap element TE wake

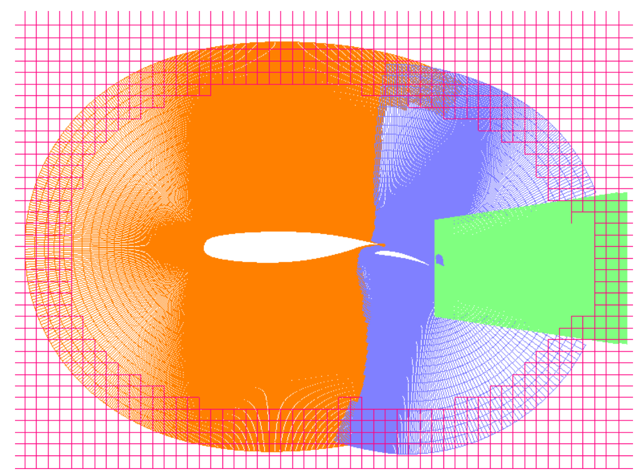

Lift improves :
0.14% < 0.4% exp_accuracy
Drag improves:
1.48% < 2.0% exp_accuracy

	C_l	C_d
Baseline	2.4321	0.0270
Grid refinement for shear layer	2.4371	0.0267
Wake layer grid addition	2.4325	0.0268
Both grid addition	2.4356	0.0266
Experimental	2.42	0.0229

Grid Connectivity Study

α=6°, Re = 2.51E6, and Ma = 0.185, Steady State

- PEGASUS: Outside of OVERFLOW

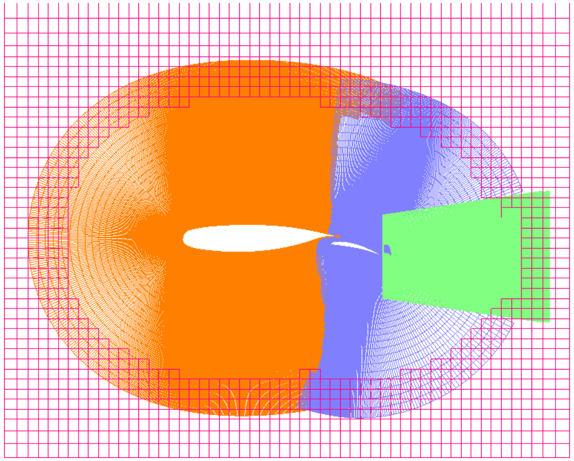

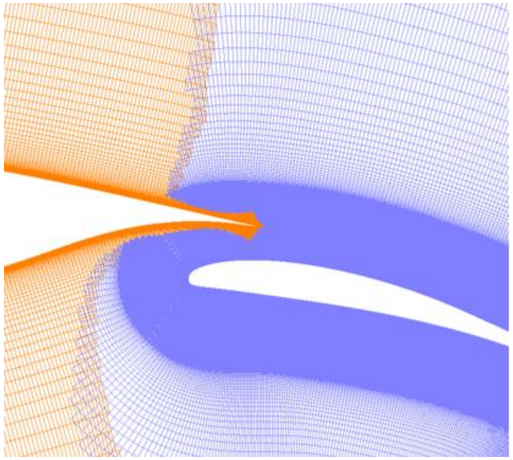

- Domain Connectivity Function (DCF): Built-in in OVERFLOW

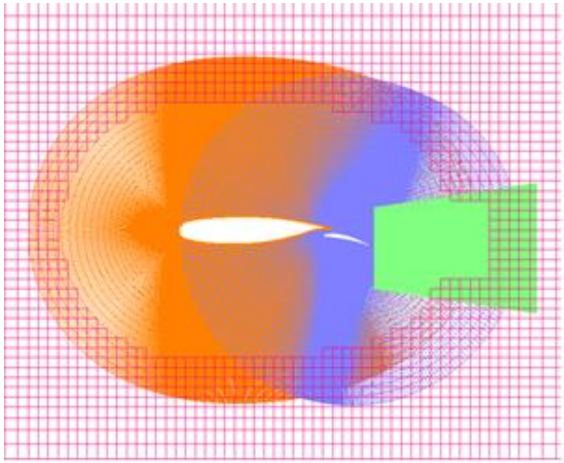

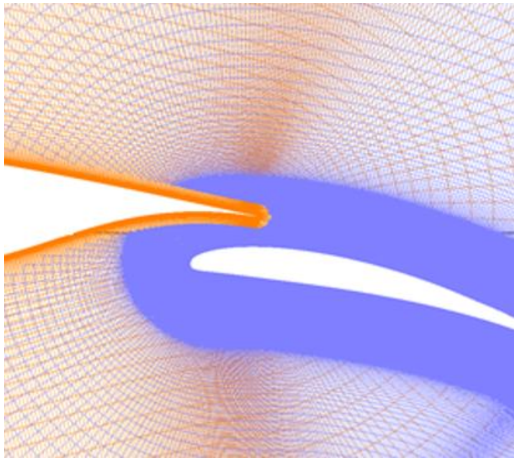

Grid Connectivity Study

α=6°, Re = 2.51E6, and Ma = 0.185, Steady State

	C_l	ΔC_l% error	C_d	ΔC_d% error
Pegasus	2.436	0.65%	0.0266	%16.2
DCF	2.413	0.30%	0.0289	%26.2

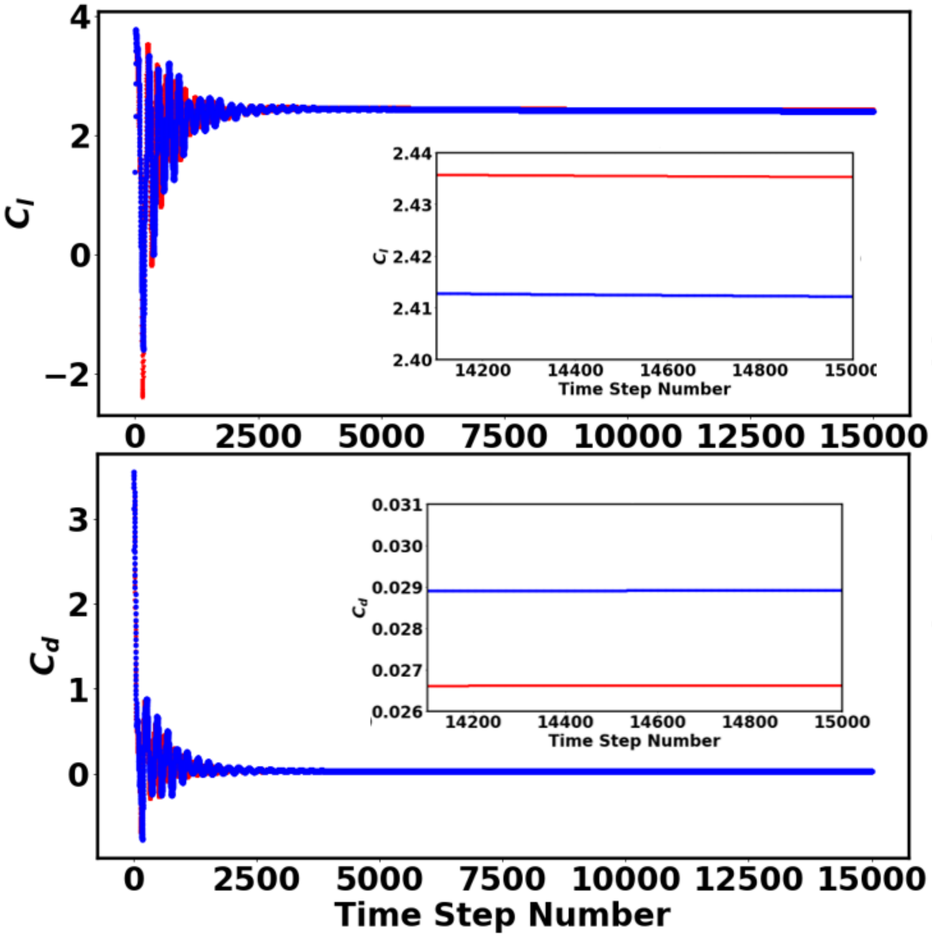

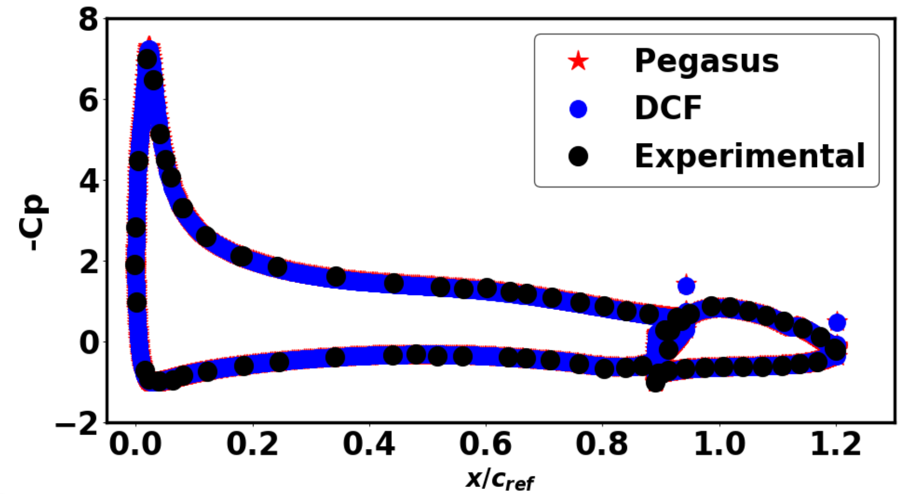

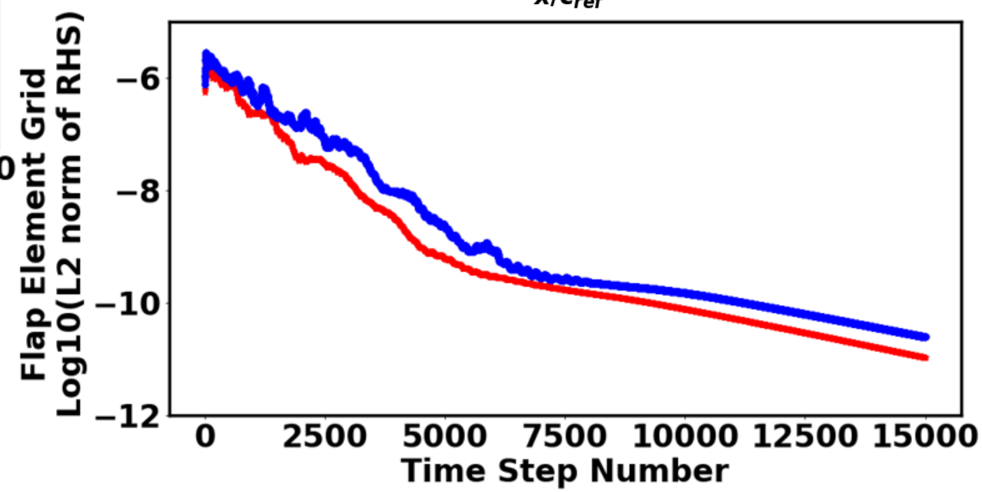

DCF is the selected overset tool

Grid Modification

α=6°, Re = 2.51E6, and Ma = 0.185, Steady State

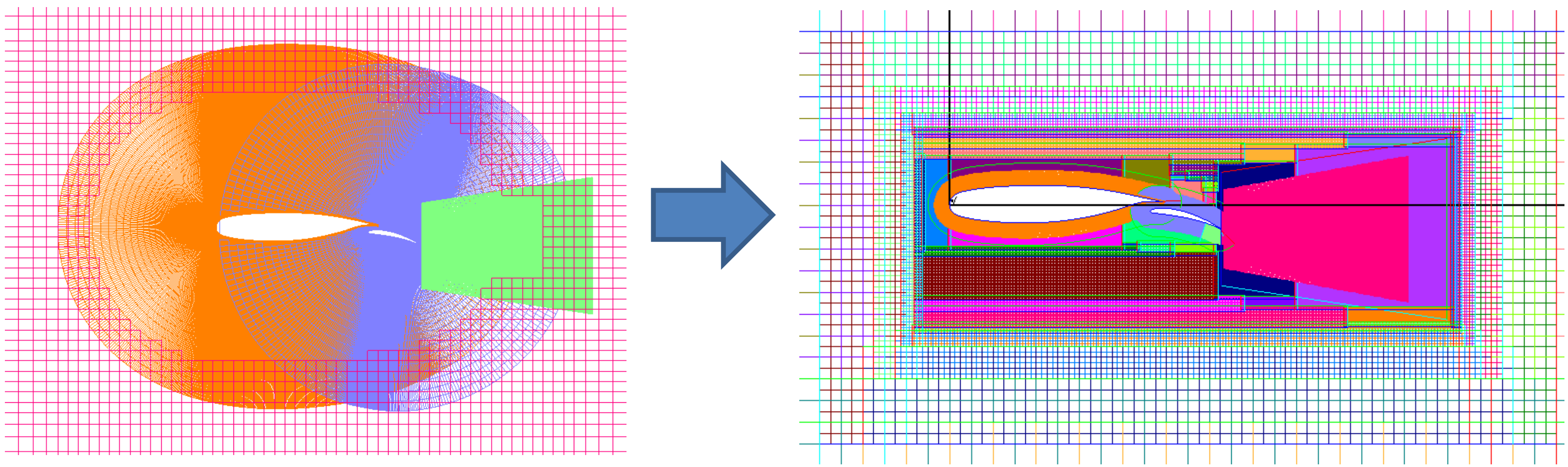

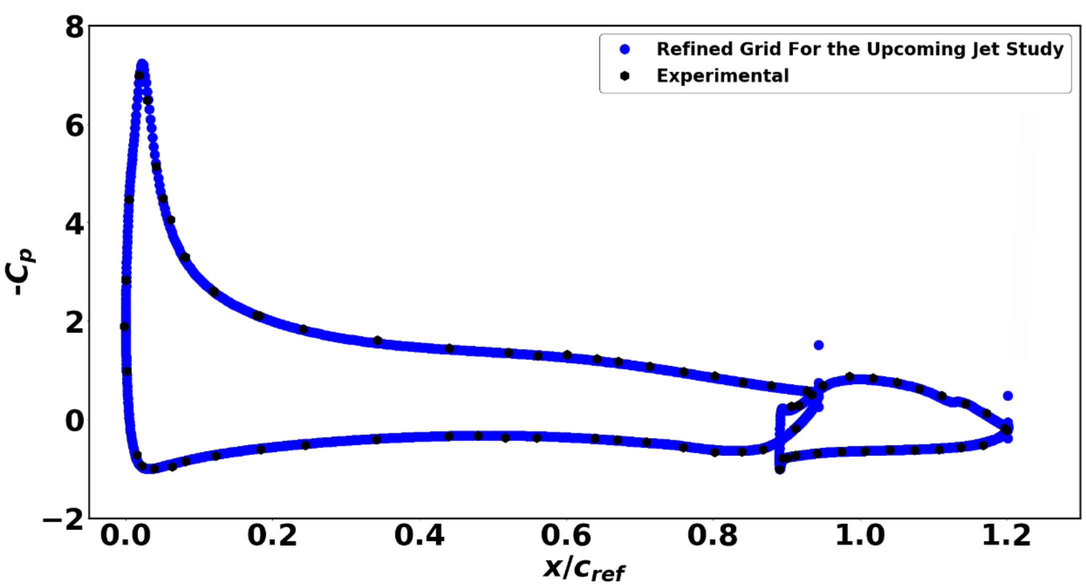

	C_l	ΔC_l% error	C_d	ΔC_d% error
Final Grid	2.416	0.16%	0.0284	24.0%

Solver Study

α=6°, Re = 2.51E6, and Ma = 0.185, Steady State

	LHS	RHS	Clock Time[min]	C_l	ΔC_l% error	C_d	ΔC_d% error
00	ARC3D approx. factor.	Central diff.	27.30	2.4159	0.16%	0.0284	24.0%
20	ARC3D diag. approx. factor.	Central diff.	16.38	2.4159	0.16%	0.0284	24.0%
60	SSOR	Central diff.	39.11	2.4159	0.16%	0.0284	24.0%
26	ARC3D diag. approx. factor.	HLLE++ upwind	23.21	2.4276	0.31%	0.0286	24.9%
66	SSOR	HLLE++ upwind	42.14	2.4276	0.31%	0.0286	24.9%

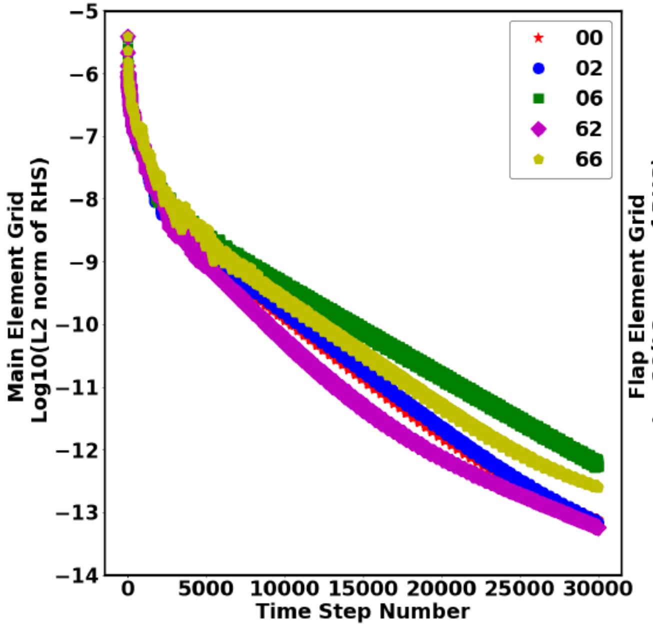

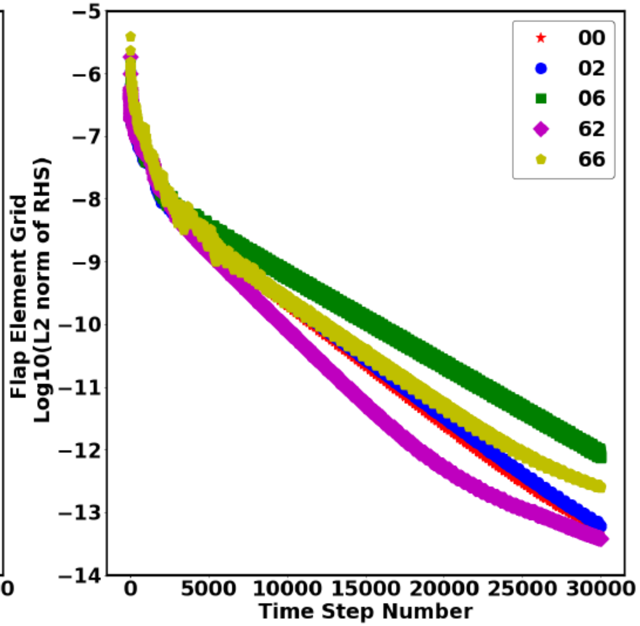

Solver Study

α=6°, Re = 2.51E6 and Ma = 0.185, Steady State

$$\frac{\partial \vec{q}}{\partial t} + \frac{\partial \vec{E}}{\partial \xi} + \frac{\partial \vec{F}}{\partial \eta} + \frac{\partial \vec{G}}{\partial \zeta} = 0$$

$$\boldsymbol{\xi} = \boldsymbol{\xi}(x,y,z,t)$$
$$\boldsymbol{\eta} = \boldsymbol{\eta}(x,y,z,t)$$
$$\boldsymbol{\zeta} = \boldsymbol{\zeta}(x,y,z,t)$$

$$q = \begin{bmatrix} \rho \\ \rho u \\ \rho v \\ \rho w \\ \rho e_0 \end{bmatrix}$$

A ≈ LHS x

$$\left[I + \frac{\Delta t}{(1+\theta)\Delta\tau} + \frac{\Delta t}{1+\theta}\left(\partial_\xi A + \partial_\eta B + \partial_\zeta C\right)\right] \Delta q^{n+1,m+1} = -\left[\left(q^{n+1,m} - q^{n,m}\right) - \frac{\theta}{1+\theta}\Delta q^n + \frac{\Delta t}{1+\theta} RHS^{n+1,m}\right]$$

b

Ax = b

$$\left[I + \frac{\Delta t}{1+\theta}\partial_\xi A\right]\left[I + \frac{\Delta t}{1+\theta}\partial_\eta B\right]\left[I + \frac{\Delta t}{1+\theta}\partial_\zeta C\right] \Delta q^{n+1,m+1} = -\left[\left(q^{n+1,m} - q^{n}\right) - \frac{\theta}{1+\theta}\Delta q^n + \frac{\Delta t}{1+\theta} RHS^{n+1,m}\right] + Error$$

ARC3D approx. factor.

$$Error = \left[\left(\frac{\Delta t}{1+\theta}\right)^2 \left(\partial_\xi A \partial_\eta B + \partial_\xi A \partial_\zeta C + \partial_\eta B \partial_\zeta C\right) - \left(\frac{\Delta t}{1+\theta}\right)^3 \left(\partial_\xi A \partial_\eta B \partial_\zeta C\right)\right] \Delta q^{n+1,m+1}$$

$$\frac{\partial \vec{q}}{\partial t} + \frac{\partial \vec{E}}{\partial \xi} + \frac{\partial \vec{F}}{\partial \eta} + \frac{\partial \vec{G}}{\partial \zeta} = 0$$

$\boldsymbol{\xi} = \boldsymbol{\xi}(x,y,z,t)$

$\boldsymbol{\eta} = \boldsymbol{\eta}(x,y,z,t)$

$\boldsymbol{\zeta} = \boldsymbol{\zeta}(x,y,z,t)$

$$q = \begin{bmatrix} \rho \\ \rho u \\ \rho v \\ \rho w \\ \rho e_0 \end{bmatrix}$$

$A \approx LHS$ x

$$\left[I + \frac{\Delta t}{(1+\theta)\Delta\tau} + \frac{\Delta t}{1+\theta}\left(\partial_\xi A + \partial_\eta B + \partial_\zeta C\right)\right]\Delta q^{n+1,m+1} = -\left[\left(q^{n+1,m} - q^{n,m}\right) - \frac{\theta}{1+\theta}\Delta q^n + \frac{\Delta t}{1+\theta} RHS^{n+1,m}\right]$$

b

First order time diff: $\theta = 0$

Second order time diff: $\theta = 0.5$

Add pseudo time for time-accurate $\left(\frac{\Delta t}{(1+\theta)\Delta\tau}\right)$

Ax = b

$$A = X_A \Lambda_A X_A^{-1}$$

$$B = X_B \Lambda_B X_B^{-1}$$

$$C = X_C \Lambda_C X_C^{-1}$$

$$X_A\left[I + \frac{\Delta t}{1+\theta}\partial_\xi \Lambda_A\right] X_A^{-1} X_B \left[1 + \frac{\Delta t}{1+\theta}\partial_\eta \Lambda_B\right] X_B^{-1} X_C \left[I + \frac{\Delta t}{1+\theta}\partial_\zeta \Lambda_C\right] X_C^{-1} \Delta q^{n+1,m+1} = -\left[\left(q^{n+1,m} - q^n\right) - \frac{\theta}{1+\theta}\Delta q^n + \frac{\Delta t}{1+\theta} RHS^{n+1,m}\right] + Error$$

Solver Study

α=6°, Re = 2.51E6 and Ma = 0.185, Steady State

UCDAVIS COLLEGE OF ENGINEERING

$$\frac{\partial \vec{q}}{\partial t} + \frac{\partial \vec{E}}{\partial \xi} + \frac{\partial \vec{F}}{\partial \eta} + \frac{\partial \vec{G}}{\partial \zeta} = 0$$

$$\boldsymbol{\xi} = \boldsymbol{\xi}(x,y,z,t)$$
$$\boldsymbol{\eta} = \boldsymbol{\eta}(x,y,z,t)$$
$$\boldsymbol{\zeta} = \boldsymbol{\zeta}(x,y,z,t)$$

$$q = \begin{bmatrix} \rho \\ \rho u \\ \rho v \\ \rho w \\ \rho e_0 \end{bmatrix}$$

$A \approx LHS$ x

$$\left[I + \frac{\Delta t}{(1+\theta)\Delta\tau} + \frac{\Delta t}{1+\theta}\left(\partial_\xi A + \partial_\eta B + \partial_\zeta C\right)\right]\Delta q^{n+1,m+1} =$$
$$-\left[\left(q^{n+1,m} - q^{n,m}\right) - \frac{\theta}{1+\theta}\Delta q^n + \frac{\Delta t}{1+\theta} RHS^{n+1,m}\right]$$

b

Ax = b

$$\Delta q_{j,k,l}^{mm+1} = \left(1 - \Omega_{ssor}\right)\Delta q_{j,k,l}^{mm} + \Omega_{ssor}\left(\overline{RHS} - \overline{A}_L \Delta q_{j-1,k,l}^{mm-1} - \overline{A}_R \Delta q_{j+1,k,l}^{mm-1}\right.$$
$$\left. - \overline{B}_L \Delta q_{j,k-1,l}^{mk1} - \overline{B}_R \Delta q_{j,k+1,l}^{mk2} - \overline{C}_L \Delta q_{j,k,l-1}^{ml1} - \overline{C}_R \Delta q_{j,k,l+1}^{ml2}\right)$$

Forward Sweep

$$mk1 = mm + 1$$
$$mk2 = mm$$
$$ml1 = mm + 1$$
$$ml2 = mm$$

Backward Sweep

$$mk1 = mm$$
$$mk2 = mm + 1$$
$$ml1 = mm$$
$$ml2 = mm + 1$$

Turbulence Model Study

α=6°, Re = 2.51E6, and Ma = 0.185, Steady State

UC DAVIS COLLEGE OF ENGINEERING

Experiment accuracy: Cl: ±0.4% Cd: ±2.0%

Turbulence Model	Clock Time[min]	C_l	ΔC_l% error	C_d	ΔC_d% error
SA	16.38	2.4159	0.16%	0.0284	24.0%
SST	32.08	2.3946	1.05%	0.0301	31.4%
SST with Langtry-Menter transition	52.35	2.4609	1.69%	0.0260	13.5%

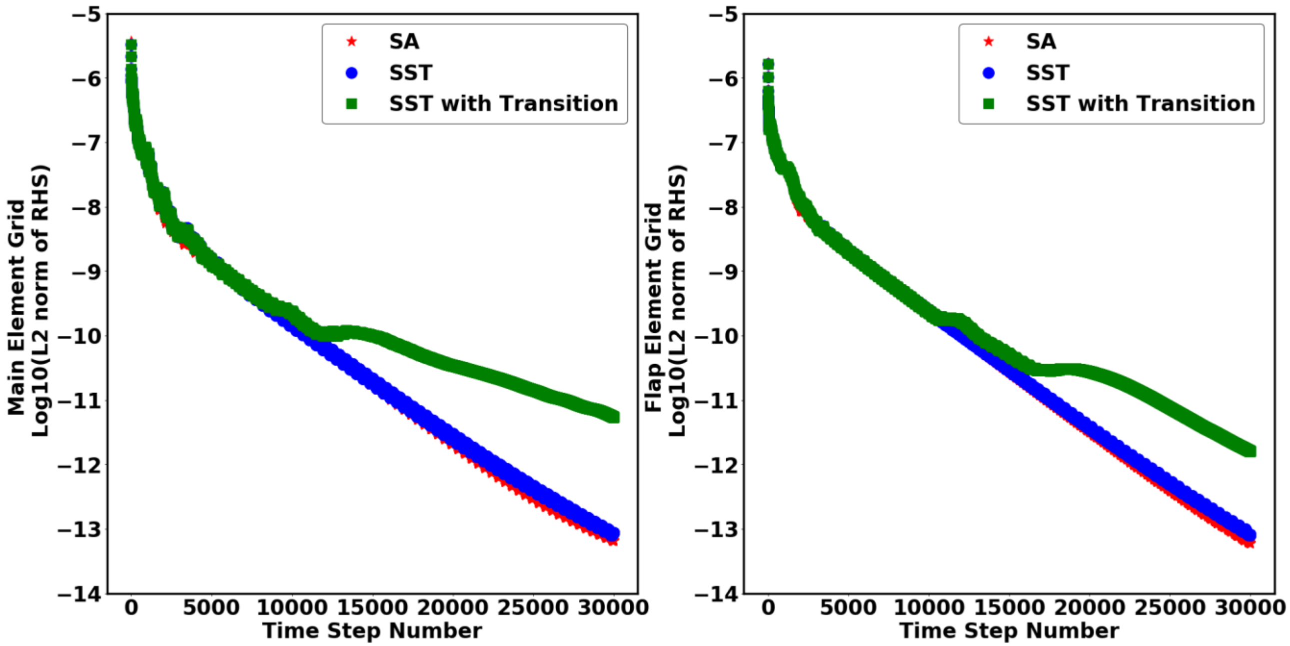

Future studies will implement SST with transition

Microjet vs. Microtab Study

α=6°, Re = 2.51E6, and Ma = 0.185, Steady State

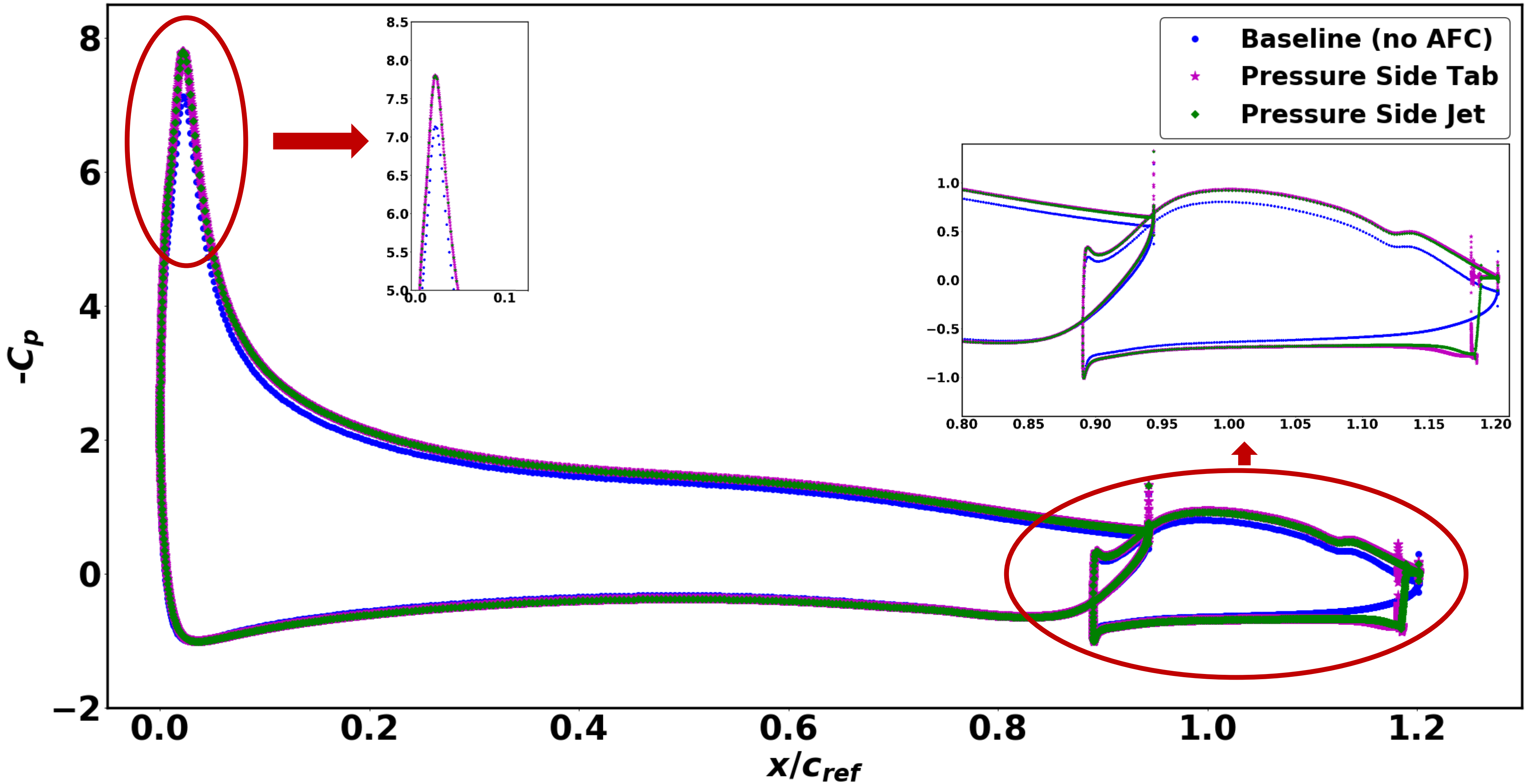

Microjet Momentum Coefficient

α=6°, Re = 2.51E6, and Ma = 0.185

- C_μ range: 0.0004-0.04 for the jet exit $h_j = 0.005$
  - $C_\mu < 0.01$ converged with steady state simulations
  - $C_\mu \geq 0.01$ required time-accurate simulations

Steps:

1. Steady state: converge the baseline airfoil (no microjet)
2. Steady state: turn on the microjet
3. If not converged, run time-accurate

$$DT = \frac{\Delta T}{\frac{L}{U_\infty}} \quad where \quad \Delta T = \frac{\frac{1}{f}}{100} \rightarrow need\ f$$

$$S_t = \frac{f.D}{U_\infty} \rightarrow \frac{1}{f} = \frac{D}{S_t U_\infty}$$

$$DT = \frac{D}{100 L S_t}$$

D = Height of equivalent micro-tab
St = .21 (White 2008)
L = 1
DT = 0.000234

Effect on Pressure Profiles

α=11°, Re = 2.51E6 and Ma = 0.185, C_μ = 0.01

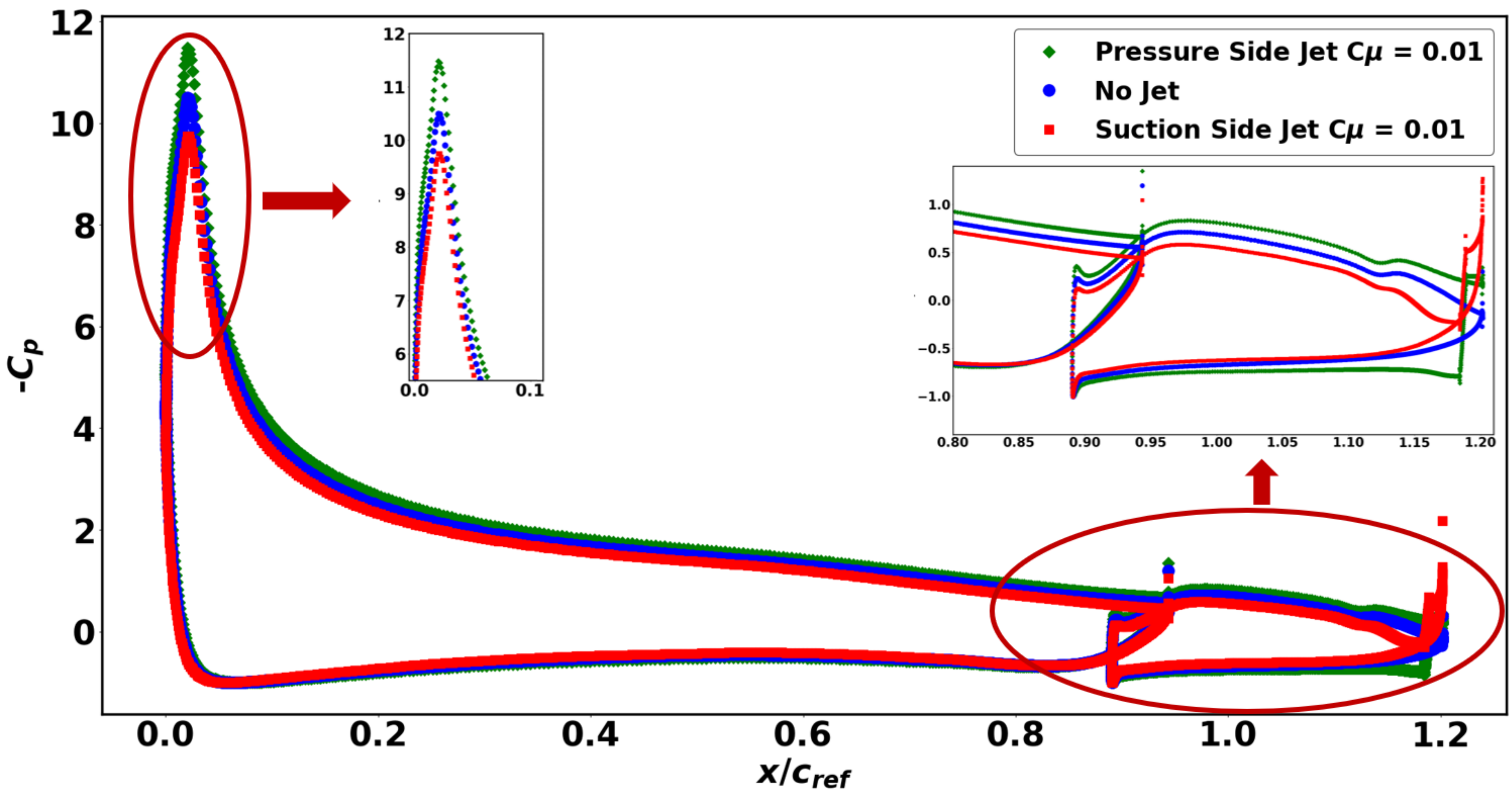

dp/dx line plot is desired

Motivation

- High-lift systems have significant impact on sizing, economics and safety of transport airplanes
  - $L/D\ and\ C_{lmax}$ 1.0% can increase passenger count by 14-22
  - $V_s = [\frac{W}{S}\frac{2}{\rho C_{Lmax}}]^{0.5}$
  - $V_{TO} = 1.2V_s = 1.2[(\frac{W}{S})_{TO}\frac{2}{\rho C_{Lmax}}]^{0.5}$
  - $TOP = (\frac{W}{S})_{TO}\frac{1}{C_{Lmax}}(\frac{W}{S})_{TO}\frac{1}{\sigma} \quad \sigma = \frac{\rho_{TO}}{\rho_{SL}}$

$STO = 20.9(TOP) + 87\sqrt{TOP(\frac{T}{W} - \frac{1}{\frac{L}{D}})}$ T/W: thrust-to-weight f(altitude)

- high-lift system accounts for somewhere
- between 6% and 11% (p

Summary I

- The high lift system is a critical component of transport airplanes with small changes in its aerodynamic performance having a large impact on the overall performance of the airplane. E.g. for a large twin-engine civil transport jet (Boeing, 1993):
  - Takeoff/landing
    - $\Delta(L/D)$ = +1% results in an increase in airplane payload of 2,800 lb assuming second-segment climb limited performance
    - $\Delta C_{L_{max}}$ = +1.5% results in an increase in airplane payload of 6,600 lb at fixed approach speed
    - ΔC_L = +0.10 reduces required landing gear height results in a reduction in airplane empty weight of 1,400 lb
- This study focuses on the application of active flow control (AFC) for airplane high lift systems.
- The AFC concept studied is the microjet to control the aerodynamic loads and performance of airplane high lift systems.
- The microjet involves a nominally-orthogonal jet injecting momentum normal to the airfoil surface near the flap trailing edge, where it modifies the trailing edge flow and, thereby, the airfoil circulation.

Summary II

- The study proposes the use of CFD to study achievable gains in the aerodynamic performance of the high lift system
- OVERFLOW is the CFD flow solver applied for this study. It uses structured overset grids to simulate fluid flow, and is being used on a wide range of aeronautical research projects in government labs, industry, and academia.
- The CFD method was validated for a two-element high lift airfoil (NLR7301) for which benchmark experimental results are available in the open literature.
- The initial 2-D CFD results for the two-element high lift airfoil demonstrate the feasibility of the microjet concept for high lift system performance enhancement and aerodynamic load control.
  - Ability to shift lift curve up (blowing on pressure side of flap) and down (blowing on suction side of flap) in linear regime of the curve
  - Modify the stall angle and maximum lift coefficient of the multi-element airfoil
  - Improve lift-to-drag ratio of the multi-element airfoil

Next Steps II

- 3-D Reynolds-averaged Navier-Stokes on realistic airplane wing.
  - High lift version of the NASA Common Research Model (CRM). Extensively studied in a wide range of configurations by a large number of researchers.
  - Validate CFD results for the baseline high lift configuration
  - Apply findings of preceding 2-D and 3-D studies for microjet layout on CRM and study effects on airplane lift, drag, moment, and flap load, hinge moment.
- Overall system considerations for CRM configuration
  - Blowing power requirements
  - Mass flow requirements
  - Impact on overall airplane system

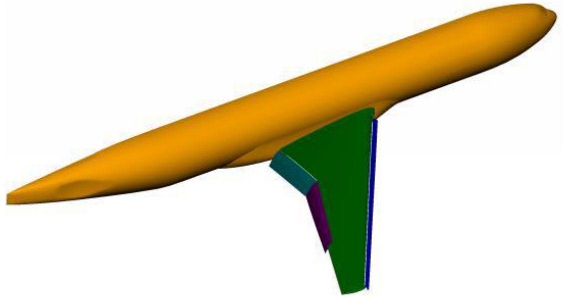

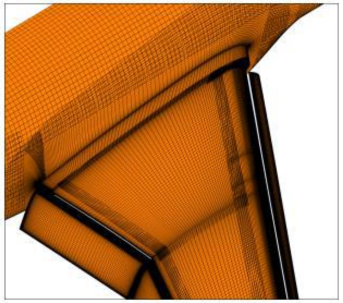

Future Studies